Università degli Studi di Napoli “Federico II”
Facoltà di Scienze Matematiche Fisiche e Naturali

Search for $\nu_\mu \leftrightarrow \nu_\tau$ oscillations in a short baseline experiment

Luca Scotto Lavina

Ph.D. in Physics
Dottorato di Ricerca in Fisica Fondamentale ed Applicata
XVII Ciclo

Supervisori:
Prof. Paolo Strolin
Dott. Giovanni De Lellis

Coordinatore:
Prof. Arturo Tagliacozzo

Contents

Introduction

Neutrino oscillations were first introduced in 1957 by B. Pontecorvo. This phenomenon occurs if neutrinos have masses and if they mix among each other, in close analogy to the experimentally observed mixing in the quark sector. In the last 30 years some unexpected experimental observations of the solar and atmospheric neutrinos were interpreted as hints on favor of neutrino oscillation. There is now a clear evidence of neutrino oscillation: experimental proofs come from more systematic studies of solar and atmospheric neutrinos and recently also from studies on neutrinos produced by accelerators and reactors.

The Standard Model is constructed to give massless neutrinos according to the failure of observing experimentally right-handed neutrinos. The value of the neutrino mass can be directly probed by experiments on neutrinoless double beta decay or tritium beta decay, but so far only upper limits have been fixed.

As an interference effect, the search of neutrino oscillations is the only way to investigate even very small differences of neutrino masses. At least two different frequencies of oscillations are found. The solar neutrino frequency was first discovered by R.Davis, in a research of Brookaven National Laboratory that spanned from 1967 to 1985: only one third of solar (electronic) neutrinos produced by sun and predicted by solar models were detected in the Homestake mine. In 2001, SNO experiment gives a solar model independent proof of ν_e disappearance, explaining it as a $\nu_e \leftrightarrow \nu_\mu$ oscillation. Togheter with CHOOZ and KamLAND experiments, a measurement of Δm^2_{12} and $sin^2 2\theta_{12}$ is done. The second frequency was first observed in 1998 by Kamiokande experiment by observing muonic neutrinos produced in the atmoshpere: the number of upward-moving ν_μ neutrinos, which travel a long distance through the entire Earth, was smaller than number of downward-moving, which travel a short distance from the upper atmosphere. With SuperKamiokande and K2K experimental results, this is now explained as a $\nu_\mu \leftrightarrow \nu_\tau$ oscillation enhanced by the presence of the matter.

The CHORUS (CERN Hybrid Oscillation Research ApparatUS) experiment was designed to search for $\nu_\mu \rightarrow \nu_\tau$ oscillations aiming at high sensitivity for small mixing angle in the region of large value of Δm^2: up to $sin^2 2\theta_{\mu\tau} \simeq 2 \cdot 10^{-4}$ for $\Delta m^2 \geq 50 - 100\ eV^2$ according to the proposal. The choice to explore with

high sensitivity that region of parameter space was suggested by the hypotesis that the neutrino mass could contribute to the solution of the dark matter puzzle.

CHORUS is an appearance experiment, it searches for ν_τ neutrinos in the almost pure ν_μ SPS-CERN neutrino beam through the direct observation of τ decays in ν_τ *CC* interactions. The short τ lifetime suggested to the use of nuclear emulsions to detect its decay. The detector is composed of a nuclear emulsion target and electronic detectors.

The CHORUS experiment performed already a first analysis of data. No signal was found, then a region of parameters space was excluded [23]. Thanks to several improvements in data taking, the CHORUS Collaboration has made a re-analysis if the data, aiming at the design goal.

This work is actually the re-analysis of the data focused on the $\nu_\mu \rightarrow \nu_\tau$ search. All the analysis chain is simulated and the efficiencies for all the τ decay channels are obtained. Then a detailed analysis of all the background sources is performed. It mainly consists of two components. One comes from the decay of short lived particles as charm or strange hadrons, the other comes from the hadrons interaction without wisible signs of the nucleus recoil or break-up in emulsion. To enhance the sensitivity to the τ detection, more background reduction criteria are studied and precise measurements in emulsions are performed. Combining the efficiencies and the background evaluation, the CHORUS sensitivity to the neutrino oscillations is calculated. Finally, using observed data, a limit of $\nu_\mu \rightarrow \nu_\tau$ oscillation is presented.

In the chapter 1 it is shown a general introduction to the neutrino oscillations phenomenology and the most updated results about neutrino masses and mixing matrix. In the chapter 2 a brief description of the CHORUS experimental layout is done. In the chapter 3 it is described the location procedure of neutrino interaction. It is also described the simulation chain used to evaluate the detection efficiencies. Chapter 4 is devoted to the analysis.

Chapter 1

Neutrino oscillations

There is by now convincing evidence, from the experimental study of atmospheric and solar neutrinos, for the existence of at least two distinct frequencies of neutrino oscillations. This in turn implies non-vanishing neutrino masses and a mixing matrix, in analogy with the quark sector and the CKM matrix. The absolute neutrino mass scale can be probed by non-oscillatory neutrino experiments, like the study of tritium beta decay or the search of neutrinoless beta decay. These experiments currently provide upper limits on neutrino masses. Recently, also astrophysical and cosmological observations have started to provide indirect upper limits. The most recent results put limits around few eV or less.

The smallness of neutrino masses is probably related to the fact that neutrinos are completely neutral (i.e. they carry no charge which is exactly conserved) and are Majorana particles with masses inversely proportional to the large scale where lepton number conservation is violated. Majorana masses can arise from the *see-saw* mechanism, in which case they are related to the Dirac masses. The relation with the non-conservation of leptonic number L could be connected with Grand Unified Theories (GUT's). So neutrino masses and mixings can represent a probe into the physics at GUT energy scales and offers a different perspective on the flavour problem and the origin of fermion masses.

There are also direct connections with important issues in astrophysics and cosmology as for example baryogenesis through leptogenesis [1] and the possibly non-negligible contribution of neutrinos to hot dark matter in the Universe [2].

In this chapter, a theoretical introduction to neutrino oscillations is presented, using the three-flavour mixing framework. Then, the most recent experimental results are shown, showing how they measured or constrained some of the neutrino oscillation parameters.

1.1 The neutrino mixing

The three-flavour mixing framework is widely used since two distinct neutrino oscillation frequencies have already been confirmed by several experiments. This scenario is welcome, since the measurement of the Z^0 decay amplitude performed at LEP [3] demonstrates that only three weakly interacting lepton families exist. However, it's also possible to introduce the presence of sterile neutrinos, which don't interact with ordinary matter, but their presence increases the number of oscillation parameters.

Neutrino oscillations can occur if the flavour basis $\nu' \equiv (\nu_e, \nu_\mu, \nu_\tau)$, where ν_e (or ν_μ, ν_τ) is the partner of the mass and flavour eigenstate e^- (or μ^-, τ^-) in a lefthanded weak isospin SU(2) doublet, and the mass eigenstates $\nu \equiv (\nu_1, \nu_2, \nu_3)$ are different:

$$\nu' = U\nu,$$

where U is a unitary 3 by 3 mixing matrix. Given the definition of U and the transformation properties of the effective light neutrino mass matrix m_ν:

$$\nu'^T m_\nu \nu' = \nu^T U^T m_\nu U \nu$$

$$U^T m_\nu U = Diag(m_1, m_2, m_3) \equiv m_{diag},$$

we obtain the general form of m_ν (i.e. of the light ν mass matrix in the basis where the charged lepton mass is a diagonal matrix):

$$m_\nu = U^* m_{diag} U^\dagger.$$

The matrix U can be parametrized in terms of three mixing angles θ_{12}, θ_{23} and θ_{13} ($0 \leq \theta_{ij} \leq \pi/2$) and one phase ϕ ($0 \leq \phi \leq 2\pi$) [4], exactly as for the quark mixing V_{CKM}. The following definition of mixing angles can be adopted:

$$U = \begin{pmatrix} 1 & 0 & 0 \\ 0 & c_{23} & s_{23} \\ 0 & -s_{23} & c_{23} \end{pmatrix} \begin{pmatrix} c_{13} & 0 & s_{13}e^{i\phi} \\ 0 & 1 & 0 \\ -s_{13}e^{-i\phi} & 0 & c_{13} \end{pmatrix} \begin{pmatrix} c_{12} & s_{12} & 0 \\ -s_{12} & c_{12} & 0 \\ 0 & 0 & 1 \end{pmatrix}$$

where $s_{ij} \equiv sin\theta_{ij}$, $c_{ij} \equiv cos\theta_{ij}$. In addition, if ν are Majorana particles, we have the relative phases among the Majorana masses m_1, m_2 and m_3. If we choose m_3 real and positive, these phases are carried by $m_{1,2} \equiv |m_{1,2}|e^{i\phi_{1,2}}$ [5]. Thus, in general, 9 parameters are added to the Standard Model when non-vanishing neutrino masses are included: 3 eigenvalues, 3 mixing angles and 3 CP violating phases.

The neutrino oscillation experiments are not sensitive to all these parameters. To show what are the parameters that could be measured, let's derive the oscillation probability when neutrino propagates in the vacuum. Consider a neutrino beam of flavour α created at time $t = 0$ in a charged current interaction. Let's assume that it is described by a plane wave with well defined momentum $\vec{p} \equiv (p, 0, 0)$ in the x direction. The ν_α is the sum of the three different components of mass eigenstates:

$$\nu_\alpha = \sum_{i=1}^{3} U_{\alpha i} \nu_i,$$

each of them evolves in space-time with different phases, so that, at $t > 0$:

$$\nu(x,t) = \sum_{i=1}^{3} U_{\alpha i} \nu_i \cdot e^{i(px - E_i t)}.$$

Neutrinos are assumed relativistic, i.e. $|p| \gg m_i$. In this case:

$$E_i = \sqrt{p^2 + m_i^2} \simeq p + \frac{m_i^2}{2p} \simeq p$$

Using such approssimation, the neutrino wave function at time t is:

$$\nu(x,t) \simeq e^{ip(x-t)} \sum_{i=1}^{3} U_{\alpha i} \nu_i \cdot e^{-i\frac{m_i^2}{2E}t}.$$

The probability to detect the initial neutrino ν_α as a neutrino with flavour β at time t and space $x = t$ can be calculated by substituting the mass eigenstates ν_i with $\sum_{\alpha'=1}^{3} U^*_{\alpha' i} \nu_{\alpha'}$ and extracting the square of $\alpha' = \beta$ component:

$$P(\nu_\alpha \to \nu_\beta) = \left| \sum_{i=1}^{3} U_{\alpha i} \cdot e^{-i\frac{m_i^2}{2E}x} \cdot U^*_{\beta i} \right|^2 =$$

$$= \sum_i |U_{\alpha i}|^2 |U_{\beta i}|^2 + Re \sum_{i \neq j} U_{\alpha i} U^*_{\alpha j} U^*_{\beta i} U_{\beta j} e^{-i\frac{\Delta m_{ij}^2}{2E}x}$$

where $\Delta m_{ij}^2 \equiv |m_i|^2 - |m_j|^2$. Thus, neutrino oscillation experiments can measure 6 parameters:

$$\theta_{12} \qquad \theta_{23} \qquad \theta_{13} \qquad \phi \qquad \Delta m^2_{sun} \qquad \Delta m^2_{atm}$$

where:

$$\Delta m^2_{sun} = |\Delta m^2_{12}|, \qquad \Delta m^2_{atm} = |\Delta m^2_{23}|$$

The numbering 1,2,3 for Δm^2 may not coincide with the ordering from the lightest to the heaviest state. The naming *sun* and *atm* is for phenomenological and historical reasons: solar oscillations are controlled by (Δm^2_{sun},θ_{12},θ_{13}) and have been first discovered by observing a solar ν_e flux smaller than predicted by the Standard Solar Model (the so-called *solar neutrino problem*); atmospheric neutrino oscillations mainly depend on (Δm^2_{atm},θ_{23},θ_{13}) and have been first discovered by observing flux anomalies on neutrinos produced by cosmic rays in the atmosphere. Nowadays, neutrino oscillation studies are performed also using neutrinos produced by reactors or accelerators, in order to have a more direct proof on neutrino phenomenology and to perform precision measurements on oscillation parameters.

The sensitivity to a particular parameter region depends on many ingredients:

- The average energy E of neutrino beam and the distance L between the neutrino source and the detector can be tuned in order to be sensitive at a particular value of Δm^2; distances are usually splitted in short baseline (SBL) and long baseline (LBL); in the following table the order of magnitude of Δm^2 which can be probed by different kinds of experiments is shown;

Experiment	$L(m)$	$E(MeV)$	Δm^2 (eV^2)
Reactor SBL	10^2	1	10^{-2}
Reactor LBL	10^3	1	10^{-3}
Accelerators SBL	10^3	10^3	1
Accelerators LBL	10^6	10^3	10^{-3}
Atmospheric	10^7	10^3	10^{-4}
Solar	10^{11}	1	10^{-11}

- The intensity and the composition of the neutrino source affects the sensitivity to different mixing angles.

- The detector can look for a reduction of the starting neutrino flavour (disappearance experiment) or look for a particular different flavour (appearance experiment). The latter can be more effective to study a single oscillation process.

So far, we have discussed the neutrino oscillation in the vacuum. However, in order to understand the solar and the atmospheric neutrino experimental results, few words should be said about the neutrino oscillation in matter. For a complete treatment, see Ref. [6].

If neutrino propagates in the matter, as it happens when it passes through the sun or the earth, the oscillation may significantly differ from oscillation in vac-

uum. Matter can enhance neutrino mixing, and the oscillation probability in matter can be large even if the mixing angle in the vacuum is very small: this effect is known as the Mikheyev-Smirnov-Wolfenstein (MSW) effect.

This effect is due to the different interactions of the three neutrino flavours in matter. All flavours interact with the electrons, protons and neutrons through neutral current interactions while ν_e shows in addition charged current interactions with the electrons of the medium.

1.2 "Solar" neutrinos

The first experiment that obtained evidence in favor of neutrino oscillation was a solar neutrino search carried out in the Homestake mine in the early '70 [7]. A large fraction of the sun energy is produced in the reaction of the thermonuclear *pp* cycles, which also produces ν_e neutrinos. The flux of solar ν_e has been calculated in different ways in the framework of standard solar models. All these calculations agree reasonably well and their predictions are also confirmed by helioseismological measurements. After Homestake experiments, many other experiments have measured the solar neutrino flux using different techniques with different energy theresholds.

The results of such experiments report strong deficits from the predicted flux, ranging from 30% to 60%. This is the essence of the solar neutrino problem.

The Chlorine [7], Gallium [8], Super-Kamiokande (SK) [9] and Sudbury Neutrino Observatory (SNO) [10] solar neutrino experiments have convincingly established that the deficit of the observed solar ν_e flux implies new neutrino physics.

Barring sterile neutrinos and nonstandard interactions, such transitions can be naturally explained by the hypothesis of flavor oscillations in the $\nu_e \rightarrow \nu_a$ channel (ν_a being a linear combination of ν_μ and ν_τ) driven by the parameters $(\Delta m^2_{sun}, \theta_{12})$.

In particular, the charged and neutral current (CC [11] and NC [12]) data from SNO confirmed that the solar neutrino deficit is due to neutrino oscillations and not to a flaw in our modeling of the sun: the total neutrino flux is in agreement with the solar model but only about one third arrives at the Earth as ν_e while the remaining part consists of other kinds of active neutrinos, presumably ν_μ and ν_τ.

In September '03 new results have been published by the SNO Collaboration [10], obtained after adding salt to their heavy water detector in order to increase the sensitivity to the neutral current channels. The previous results have been confirmed with increased accuracy: the occurrence of ν_e transitions into a different active state ν_a have a statistical significance greater than 5σ.

The CHOOZ reactor experiment [13] looks for the $\bar{\nu}_e$ disappearance and its results are combined with the solar neutrino experiments. It also constraints the smallness of θ_{13} angle ($s_{13} < 0.10$ at 90% CL), so that it can be set to zero to a

good approximation.

The recent results from the Kamioka Liquid scintillator AntiNeutrino Detector (KamLAND) [14] have provided a crucial confirmation of the solar ν_e oscillation picture through a search for long-baseline oscillations of reactor $\bar{\nu}_e$'s. The observation of $\bar{\nu}_e$ disappearance in KamLAND has confirmed the previously favored solution in the (Δm^2_{sun},θ_{12}) parameter space, often referred to as the large mixing angle (LMA) region in the literature [15]. Moreover, the KamLAND data have basically split this region into two allowed subregions, which are referred to as LMA-I and LMA-II, following Ref. [16]. In figure 1.1 a global analysis of solar, CHOOZ and KamLAND neutrino data in the (Δm^2_{sun},θ_{12}) parameter space is shown [16].

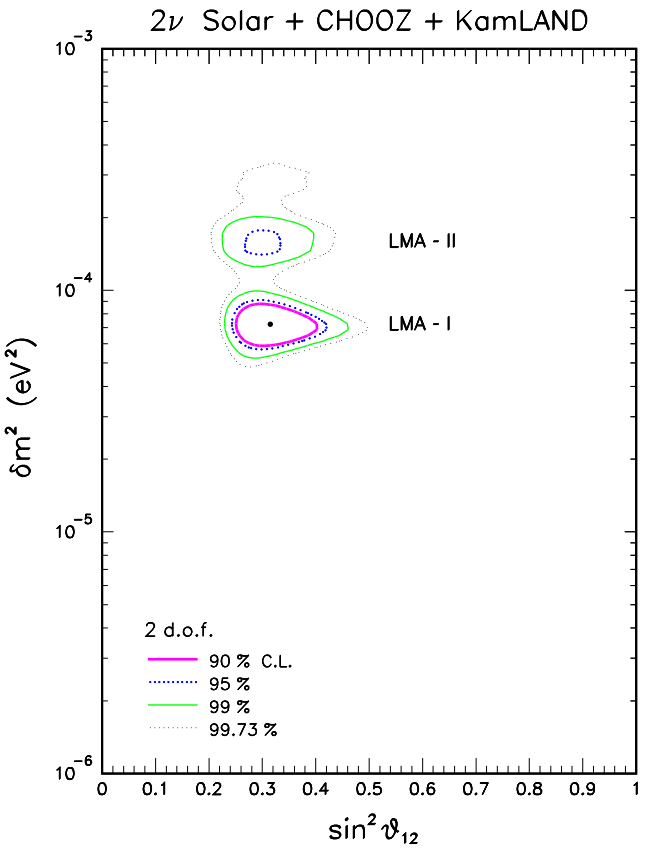

Figure 1.1: Global analysis of solar, CHOOZ and KamLAND neutrino data in the (Δm^2_{sun},θ_{12}) parameter space [16].

The LMA-I solution is clearly preferred by the data, being closer to the best

fit points of both solar+CHOOZ and KamLAND data. With just 54 initial events, the KamLAND experiment was not only able to select the LMA region as the solution to the solar neutrino problem, but could also significantly restrict the corresponding oscillation parameter space. With several hundred events expected in the forthcoming years, there are thus very good prospects to refine the parameter estimate.

Solar neutrino experiments show evidence for $\nu_e \leftrightarrow \nu_\alpha$ transitions. On the other hand, reactor experiments are used to study $\bar{\nu}_e \leftrightarrow \bar{\nu}_\alpha$ oscillations. If CPT is not conserved, these two processes should not have the same behaviour. Thus, the coincidence of the frequency found for neutrinos from the sun and for antineutrinos from reactors is consistent with the validity of CPT invariance.

As conclusion, by a combined analysis of solar+reactor neutrino experiments, the following parameters are evaluated:

$$\Delta m^2_{sun} = 6.9 \cdot 10^{-5}\, eV^2 \qquad sin^2\theta_{12} = 0.30$$

In the simplest picture, solar neutrino oscillations depend on the kinematical parameters (Δm^2_{sun},θ_{12}) and on standard dynamical MSW effects in matter.

1.3 "Atmospheric" neutrinos

Electron and muon neutrinos and antineutrinos are produced in the hadronic shower induced by cosmic rays in the atmosphere: they are called atmospheric neutrinos. They are produced mainly by the following processes:

$$\begin{array}{rcccl} p(\alpha,\ldots) + Air \rightarrow & \pi^\pm(K^\pm) & + & X & \\ & \pi^\pm(K^\pm) & \rightarrow & \mu^\pm + \nu_\mu(\bar{\nu}_\mu) & \\ & & & \mu^\pm \rightarrow e^\pm + \nu_e(\bar{\nu}_e) + \bar{\nu}_\mu(\nu_\mu) & \end{array}$$

From the reaction chain we expect that the ratio of the two flavours $N(\nu_\mu + \bar{\nu}_\mu)/N(\nu_e + \bar{\nu}_e)$ is equal to 2. The first generation of detectors, NUSEX, Soudan, IMB, Frejus and Kamiokande reported the ratio between the measured value and its predicted value based on Montecarlo simulation:

$$R = \frac{[N(\nu_\mu + \bar{\nu}_\mu)/N(\nu_e + \bar{\nu}_e)]_{Data}}{[N(\nu_\mu + \bar{\nu}_\mu)/N(\nu_e + \bar{\nu}_e)]_{MC}}$$

Some of them measured for R a value smaller than expected. The discrepancy between the observed and predicted neutrinos flavour ratio is referred to as the atmospheric anomaly. A second generation of experiments, Superkamiokande (SK) [17], Soudan-2 [18] and MACRO [19], was used to carefully study the atmospheric neutrinos. All these experiments used charged current interactions to

tag the neutrino flavour. MACRO and Soudan-2 use tracking calorimeter detectors: distinguishing between shower or tracks permits to separate events with μ or e lepton final state. SK is a water Cerenkov detector. It identifies the lepton flavor by using the Cerenkov ring which is sharp for μ and diffuse for e. All these detectors, except MACRO, are sensitive to the track direction, thus they can distinguish between upgoing and downgoing neutrinos. All these experiments confirmed the atmospheric anomaly.

Such anomaly was interpreted in terms of neutrino oscillations. To test this hypotesis, more studies were done from the SK collaboration. They ended up with signal which has been interpreted as strong evidence for neutrino oscillation.

SK results have also been independently checked by the first long-baseline KEK-to-Kamioka (K2K) [20] accelerator experiment, using SK as a target for ν_μ's produced 250 *km* away with $\langle E_\nu \rangle \sim 1.3$ *GeV*. Neutrino flavour oscillations, interpreted in terms of nonzero mass-mixing parameters $(\Delta m^2_{atm}, \theta_{23})$ in the $\nu_\mu \rightarrow \nu_\tau$ channel, provide by far the best and most natural explanation for the observed ν_μ disappearance.

Fig. 1.2 shows the joint bounds on the $(\Delta m^2_{atm}, \theta_{23})$ parameters from an analysis of SK, K2K, and SK+K2K data [16].

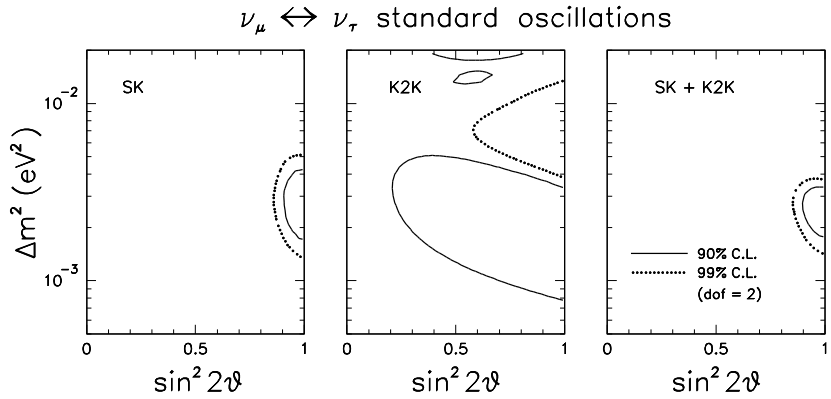

Figure 1.2: Standard oscillations in the $\nu_\mu \rightarrow \nu_\tau$ channel: bounds on the parameters $(\Delta m^2_{atm}, \theta_{23})$ from SK atmospheric data (left panel), K2K spectral data (middle panel), and their combination (right panel).

By comparing the left and right panels, the main effect of K2K appears to be the strengthening of the upper bound on Δm^2. Fig. 1.3 shows on the left the SK and SK+K2K bounds on Δm^2, when the $sin^2 2\theta_{23}$ parameter is projected (minimized) away ($sin^2 2\theta_{23} = 1$). Up to $\sim 3\sigma$, the global (SK+K2K) $\Delta\chi^2 \equiv \chi^2 - \chi^2_{min}$ function is approximately parabolic in the variable Δm^2, so that one can

define a n-standard-deviation error for this parameter by imposing the condition $\Delta\chi^2 = n^2$.

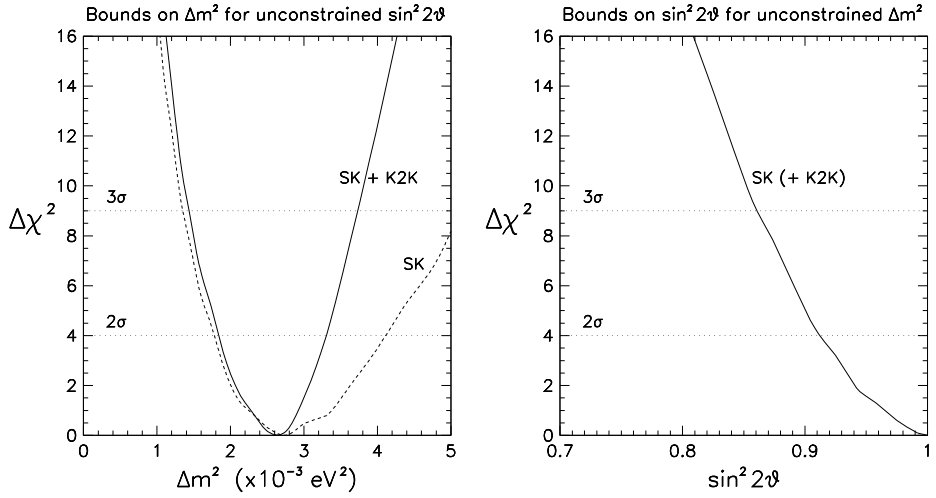

Figure 1.3: Standard oscillations in the $\nu_\mu \to \nu_\tau$ channel. On the left: bounds on Δm^2 for unconstrained $sin^2 2\theta_{23}$ from SK (dashed curve) and SK+K2K (solid curve). On the right: bounds on $sin^2 2\theta_{23}$ for unconstrained Δm^2 from SK data.

The bounds on $sin^2 2\theta_{23}$ are instead entirely dominated by SK. This is shown on the right of Fig. 1.3, where the $\sim 3\sigma$ function in terms of $sin^2 2\theta_{23}$ is reported, for Δm^2 projected (minimized) away in the SK fit ($\Delta m^2 = 2.6 \times 10^{-3}\ eV^2$). Here the addition of K2K data would insignificantly change the bounds (not shown), which thus hold for both the SK and the SK+K2K fit. Also in this case, the nearly parabolic behavior of $\Delta\chi^2$ allows to properly define a 1σ range.

Performing a parabolic fit in the 1σ range, we obtain [16]:

$$\Delta m^2_{atm} = (2.6 \pm 0.4) \times 10^{-3}\ eV^2 \qquad sin^2 2\theta_{23} = 1.00^{+0.00}_{-0.05}$$

1.4 Present knowledge on oscillation parameters

In the following table, the most updated values of neutrino oscillation parameters are shown (see Ref. [21] and [13]):

	Lower limit (3σ)	Best value	Upper limit (3σ)
$(\Delta m^2_{sun})_{LMA-I}$ $(10^{-5} eV^2)$	5.4	6.9	9.5
Δm^2_{atm} $(10^{-3} eV^2)$	1.4	2.6	3.7
$sin^2\theta_{12}$	0.23	0.30	0.39
$sin^2\theta_{23}$	0.31	0.52	0.72
$sin^2\theta_{13}$	0		0.026 $(90\%\, CL)$

According to CHOOZ, we know that θ_{13} is small. Therefore, in the ideal limit of exactly vanishing θ_{13}, the solar and atmospheric oscillations decouple and depend on two separate sets of two-flavour parameters.

For atmospheric neutrinos we have $s_{23} \sim c_{23} \sim 1/\sqrt{2}$ corresponding to nearly maximal mixing. Oscillations of muon neutrinos into tau neutrinos are favoured over oscillations into sterile neutrinos (ν_s). The conversion probability and the zenith angular distribution of high-energy muon neutrinos are sensitive to matter effects, which distinguish ν_τ from ν_s. Moreover, for conversion of ν_μ into pure ν_s, neutral current events would become up/down asymmetric. In both cases data strongly disfavour the pure sterile case. The OPERA experiment [22], which will start taking data on 2006, will be able to exclude the ν_s hypotesis by a direct observation of charged current interactions of ν_τ.

The only surviving solution to the solar neutrino problem after KamLAND and SNO-salt results is the LMA-I solution (however the LMA-II is the second best-fit point). Before KamLAND, the interpretation of solar neutrino data in terms of oscillations required the knowledge of the Boron neutrino flux, f_B. For instance, charged and neutral current data from SNO are sensitive, respectively, to $f_B\langle P_{ee}\rangle$ and to $f_B\langle\sum_a P_{ea}\rangle$ $(a = e, \mu, \tau)$, where $\langle P_{ea}\rangle$ denotes the averaged conversion probability from ν_e to ν_a. KamLAND provides a direct measurement of $\langle P_{ea}\rangle$. Beyond the impact on the oscillation parameters and a check that the solar standard model works well, the comparison among these experiments shows that the conversion of Boron solar neutrinos into sterile neutrinos is compatible with zero.

The LSND indication for a third oscillation frequency associated to one or more sterile neutrinos is not supported by any other experiment, at the moment. Moreover, LSND has not been confirmed by KARMEN. The MiniBoone experiment will soon clarify this matter. If LSND is right, we probably need one more light neutrino.

Within the three-neutrino framework, if we take maximal s_{23} and keep only linear terms in $u = s_{13}e^{i\phi}$, we find the following structure of the mixing matrix:

$$U = \begin{pmatrix} c_{12} & s_{12} & u \\ -(s_{12}+c_{12}u^*)/\sqrt{2} & (c_{12}-s_{12}u^*)/\sqrt{2} & 1/\sqrt{2} \\ (s_{12}-c_{12}u^*)/\sqrt{2} & -(c_{12}+s_{12}u^*)/\sqrt{2} & 1/\sqrt{2} \end{pmatrix}$$

where θ_{12} is close to $\pi/6$.

Given the observed frequencies, there are three possible patterns of mass eigenvalues:

$$\begin{aligned} \text{Degenerate}: &\quad |m_1| \sim |m_2| \sim |m_3| \gg |m_i - m_j| \\ \text{Inverted hierarchy}: &\quad |m_1| \sim |m_2| \gg |m_3| \\ \text{Normal hierarchy}: &\quad |m_3| \gg |m_{2,1}| \end{aligned}$$

Models based on all these patterns have been proposed and studied and all are in fact viable at present [21].

1.5 The CHORUS role

The CHORUS (CERN Hybrid Oscillation Research ApparatUS) experiment was designed to search for $\nu_\mu \to \nu_\tau$ oscillations aiming at high sensitivity for small mixing angle in the region of large value of Δm^2: up to $sin^2 2\theta_{\mu\tau} \simeq 2 \cdot 10^{-4}$ for $\Delta m^2 \geq 50 - 100\ eV^2$ according to the proposal. The choice to explore with high sensitivity that region of parameter space was suggested by the hypotesis that the neutrino mass could contribute to the solution of the dark matter puzzle [27]. In that case the sum of the mass of neutrino species should be of $\sim 15 - 65\ eV$.

In the late 80's, from the solar neutrino data, $\Delta m^2_{e,\mu} \sim 5 \cdot 10^{-6}\ eV^2$. If the see-saw mechanism is correct, the largest neutrino mass is at least two order of magnitude greater than the two others. It means that only one neutrino species contributes significantly to the dark matter: the ν_3 with a mass of $\sim 15 - 65\ eV$. The ν_3 state is mainly composed by ν_τ, thus $m_{\nu_\tau} \sim m_{\nu_3}$. Under these assumptions the squared mass splitting between ν_τ and ν_μ is $\sim m^2_\tau \geq 100\ eV^2$: therefore the idea to explore that Δm^2 region with the highest possible sensitivity in $sin^2 2\theta_{\mu\tau}$.

CHORUS is an appearance experiment, it searches for ν_τ neutrinos in the almost pure ν_μ SPS-CERN neutrino beam. The ν_τ presence is searched through the charged current reaction $\nu_\tau N \to \tau^- X$. Thus the ν_τ detection essentially consists in the τ detection. The τ short lifetime has suggested to use nuclear emulsions to distinguish its decay from the much more frequent ν_μ CC or NC interactions. The detector is composed by an emulsion target for neutrino interactions combined with an electronic detector. It is described in more detail in the next chapter.

The CHORUS experiment performed already a first analysis of data. No signal was found, then a region of parameters space was excluded [23]. Thanks to

several improvements in data taking, the CHORUS Collaboration intend to exclude a larger parameter region, aiming at the design goal. The CHORUS results, combined with the NOMAD [24] ones, will permit to explore a region not yet explored. In this thesis, we report the latest oscillation analysis of the CHORUS experiment.

Chapter 2

The CHORUS experiment

The CHORUS experiment was designed [25, 26] to search for $\nu_\mu \leftrightarrow \nu_\tau$ oscillations through the appearance of ν_τ in an almost pure ν_μ beam, aiming to explore the domain of small mixing angles down to $\sin^2 2\theta_{\mu\tau} \sim 2 \times 10^{-4}$ for mass parameters $\Delta m^2 \sim 1 eV^2$, i.e. in the region of cosmological interest [27] for the Dark Matter. This experiment represented an order of magnitude improvement over the previous generation of experiments [28]. The requirement for a pure ν_μ beam was meant to provide as many neutrinos as possible, at an average energy well above the threshold for ν_τ charged current interactions. For such purpose, the CERN Wide Band Neutrino Beam was used. It contained mainly ν_μ's ($\sim 94\%$) with a negligible contamination of prompt ν_τ, estimated as low as $3.3 \times 10^{-6} \times \nu_\mu$ CC interaction [29]. The average ν_μ beam energy was 27 *GeV* and the average distance between the neutrino beam source and the CHORUS apparatus was about 600 *m*.

The CHORUS detector is schematically shown in Fig. 2.1. It consisted of an active target of nuclear emulsion, a scintillating fibre tracker, a hadron spectrometer, a high resolution calorimeter and a muon spectrometer. The major novelty was the large-scale deployment of nuclear emulsion (770 *kg*), described afterwards in more detail. It serves both as neutrino target and as detector: the ν_τ is detected through its charged current interaction $\nu_\tau N \rightarrow \tau^- X$ and the direct observation of τ decays in emulsion. At these energies the τ travels, on average, about 1 *mm* before decaying. The emulsion target offered a sub-micron resolution for the track and vertex reconstruction in the vertex region, enough to reveal not only the decay products of the tau lepton, but also the parent track itself. After the beam exposure, the emulsions were removed and analysed with automatic microscopes. The ν_τ candidates would be confirmed by direct inspection. The only drawback of the emulsions is the absence of time information: any charged particle traversing the emulsion during the exposure leaves a track. However, the connection with electronic detectors solved this problem and also provided extra kinematic

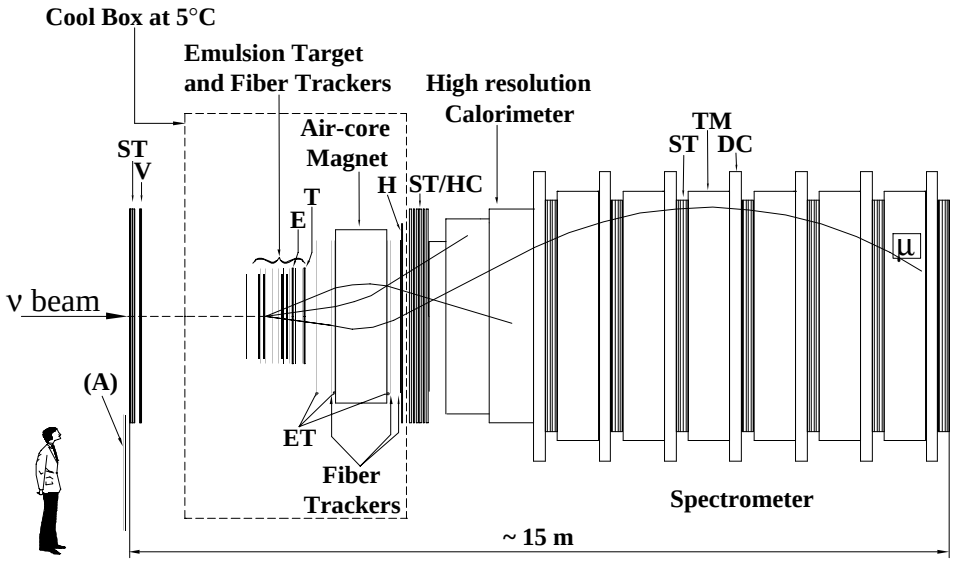

Figure 2.1: CHORUS detector layout.

informations. The use of nuclear emulsions connected with electronic detectors (called *hybrid* approach) in neutrino interaction analysis is very promising, especially with the increasing of speed and accuracy of automatic microscopes. The use of nuclear emulsions is a powerful technique for discovery experiments, in which a small number of signal events are expected.

CHORUS is well suited to directly observe the production and decay of short-lived particles. At these energies, about 6% of neutrino interactions presents charmed particle production. The charmed hadrons have a flight length comparable to the τ, so that CHORUS is suitable to study charm physics as well. Many studies and cross-sections measurements of charmed particles have been carried out so far [30]. For oscillations search, charged charmed particles constitute background. However, as we will see in chapter 4, charm plays a key role to reduce the systematic uncertainty in this analysis.

In the first part of this chapter, a short description of the neutrino beam and detector components is provided. A detailed description can be found in Ref. [31]. Then, a more detailed description of emulsion handling is presented.

2.1 The neutrino beam

The West Area Neutrino facility (WANF) of the CERN Super Proton Synchrotron (SPS) [32] provides an almost pure ν_μ beam with energy mostly above threshold for ν_τ CC interactions, thus suitable for $\nu_\mu \leftrightarrow \nu_\tau$ oscillation search in appearance mode. Protons are accelerated by the SPS up to an energy of 450 *GeV*. The proton-beryllium interaction produces mainly pions and kaons. Positive (negative) mesons are focused (defocused) by two magnetic lenses, the horn and the reflector. The mesons decay in flight in a 290 *m* long evacuated tunnel and produce neutrinos mainly via the decay channels:

$$\begin{aligned} \pi^+ &\rightarrow \mu^+\nu_\mu, \\ K^+ &\rightarrow \mu^+\nu_\mu, \\ K^+ &\rightarrow \pi^0\mu^+\nu_\mu. \end{aligned}$$

The charged leptons from the decay as well as the remaining non-decayed hadrons are absorbed in a shielding of 225 *m* iron and 144 *m* earth. Finally, a toroidal magnet defocuses not stopping muons.

The neutrino beam has an upward slope of 42 *mrad*. The detector was centred along this slope, vertically along the beam. The energy spectra of the different components of the neutrino beam intercepted by the CHORUS emulsions, as predicted by a full Montecarlo simulation of the beam line, is shown in Fig.2.2.

The neutrino exposure started in 1994 and ended in 1997. In these four years of data taking, emulsions have been exposed to the neutrino beam with an intensity corresponding to 5.06×10^{19} protons on target. CHORUS ran also in 1998, without emulsions, with a neutrino and anti-neutrino beam, using the calorimeter as target for compared analysis of cross-section νN and $\bar{\nu}N$ [33].

2.2 Detector overview

In the CHORUS experiment, nuclear emulsions are used as target for neutrino interactions. Downstream of the target region, an air core magnet provides the measurement of the hadron charge and momentum. A calorimeter measures the energy and the direction of electromagnetic and hadronic showers. The calorimeter is followed by a muon spectrometer to get the charge and the momentum of muons produced in the interactions.

The electronic detector information is used to predict the particles trajectories in the emulsions. By using automated microscopes to inspect the emulsion layers, these trajectories are followed through the emulsions until the primary neutrino interaction is found.

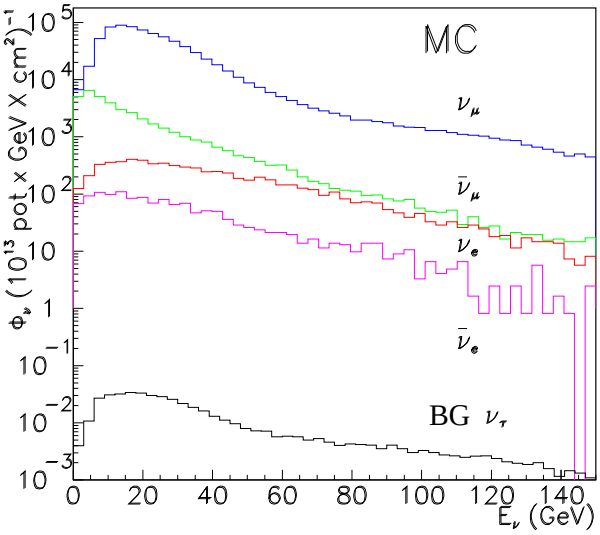

Figure 2.2: The energy spectra of the different ν components by Montecarlo simulation.

2.2.1 The trigger system

The scintillator trigger-hodoscopes E (emulsion), T (timing), H (hodoscope), V (veto) and A (anti-counter), shown in Fig. 2.3, are used to select neutrino interactions in the emulsion target and to reject background from cosmic rays, beam muons and neutrino interactions outside the target [34].

The E and T planes are installed between the emulsion target and the hadron spectrometer, whereas H is located downstream of the hadron spectrometer. The A and V planes are installed upstream of the emulsion target.

A neutrino trigger in the target region is defined by a hit coincidence in E,T and H consistent with a particle trajectory with $\tan\theta < 0.25$ with respect to the neutrino beam direction.

A veto is defined by any combination of a counter hit in the veto hodoscopes (V and A) and a hit in T, with precise timing to avoid vetoes due to backscattering of particles coming from neutrino interactions in the target.

2.2.2 Emulsion target and the tracker system

Target area consists of nuclear emulsions and electronic trackers. It is composed by two identical and contiguous part. One of these is shown in Fig. 2.4a.

Nuclear emulsions record the passage of charged particles. Along their path,

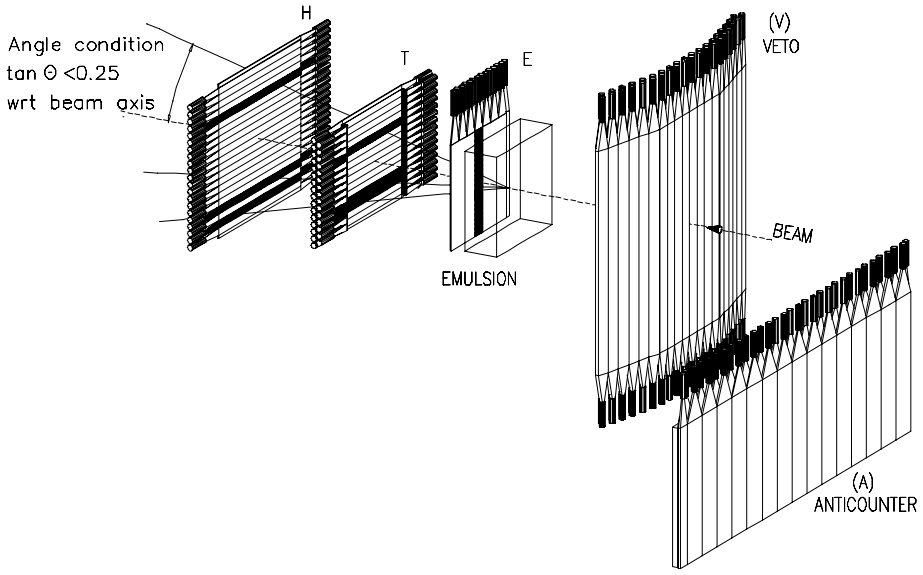

Figure 2.3: The trigger system. The neutrino trigger is defined by a hit coincidence in E,T and H planes in anti-coincidence with the A and V veto.

charged particles produce ionisation which makes the silver crystals developable. After development, a three-dimensional image can be reconstructed by the produced silver grains. The emulsion target is divided into four stacks, transversally consisting of eight modules, having a surface area of $1.42 \times 1.44\ m^2$ and a thickness of about 28 *mm*. Each stack module is composed by 36 emulsion sheets (*plates*) (Fig. 2.4b), piled up in close contact with each other and vacuum packed. In each plate, emulsion gel with a thickness of 350 μm is poured onto both faces of a 90 μm thick tri-acetate cellulose foil. Along the beam direction, the emulsions amount to about 4 radiation lengths and 0.3 interaction lengths.

Special interface emulsion sheets, Changeable Sheet (CS) close to the electronic detector and Special Sheet (SS) close to the emulsion stack, reconstruct the trajectories of the charged particles with very high precision for the location of the vertex position. The interface sheets are composed by a 800 μm thick plastic base and two emulsion layers of 100 μm. The different emulsion and base thicknesses of the CS/SS sheets with respect to the bulk plates are due to the ne-

cessity to maximise the angular resolution to match the electronic detector track with the emulsion track. In fact, the interface sheets have a larger level arm and less distortion due to the smaller thickness. In order to provide favourable background conditions for the recognition of the predicted tracks in the emulsions, in the 1994-95 data taking the changeable sheets were replaced every three to six weeks during the data taking. Owing to the good accuracy achieved, in 1996-97 exposure only one change per year was found necessary.

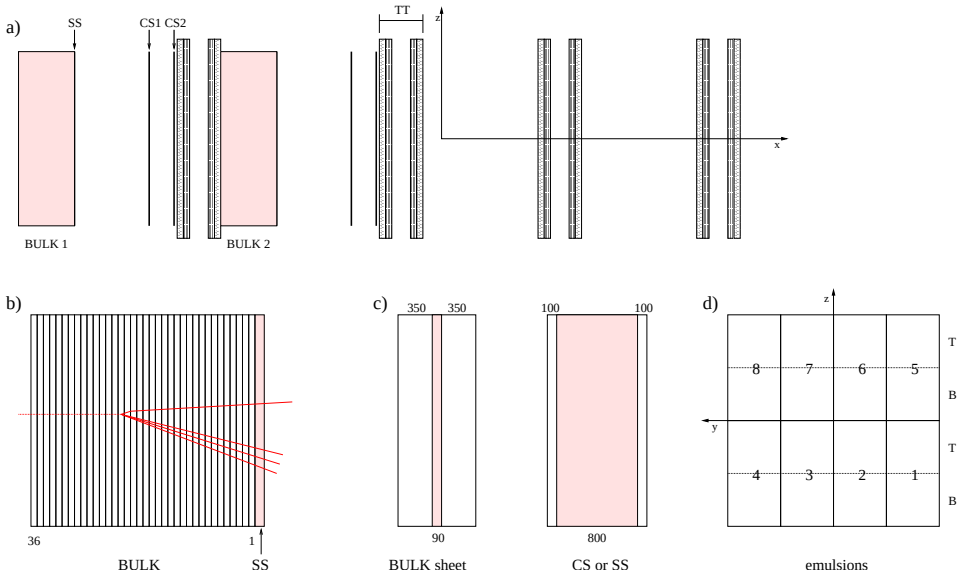

Figure 2.4: Sketch of emulsion target. The neutrino goes through the *x* direction. The longitudinal size is not proportional to the transversal one. a) It is shown one of two contiguous half targets, composed of two emulsion bulks, two SS, four CS, and eight scintillating fibre trackers; b) bulk target (36 emulsion sheets) and the attached SS; c) CS and SS have different proportions emulsion/base respect to the bulk sheets; d) All emulsions are transversally divided in eight modules. Each module is conceptually divided in two semi-modules, top and bottom.

The purpose of the electronic trackers is to reconstruct the event and to predict the impact point and slope of tracks in these interface sheets, with an accuracy good enough for the scanning to uniquely identify this track among those integrated [35]. CHORUS used planes of scintillating fibres. Each tracker module consists of four projection planes (Y,Z, and $Y^{\pm}$, $Z^{\pm}$ rotated by 8^o relative to Y,Z). The prediction accuracy in CS was measured as $\sigma \sim 150$ μm in position and $\sigma \sim 2.5$ mrad in angle [36].

2.2.3 The hadron spectrometer

For the τ search in the hadronic decay channel, the rejection of background from charm production relies critically on the ability to determine the charge of hadrons. A second source of background are the so-called *white kinks*: elastic or inelastic hadron interactions which show no visible recoil nor delta rays or Auger electrons and which in the emulsion cannot be distinguished from a decay. To reduce this kind of background, the measurement of hadron momenta must be precise enough to reject decay topologies with a low-momentum secondary or corresponding to small transverse momentum. The hexagonal spectrometer, consisting of an air-core magnet and scintillating fibre trackers, was deputed to the hadron momentum measurement [37].

The magnet produced a toroidal field of $0.12\ T$ and it was pulsed synchronously with the neutrino beam. The field strength had no radial dependence and it was parallel to the outer side of the triangle. Three fibre trackers, called Diamond Tracker modules (DT), one upstream and two downstream from the air-core magnet measured the trajectory curvature. The momentum resolution $\Delta P/P$ of the magnet tracker results from the quadratic combination of two terms: a constant term from multiple scattering and a term proportional to particle momentum which reflects the measurement accuracy. The measured resolution, showed also in Fig. 2.5 was:

$$\frac{\Delta P}{P} = 22\% + 3.5\% \frac{P}{GeV/c} \tag{2.1}$$

The hexagonal spectrometer resolution was sufficient for the CHORUS analysis, but unfortunately the momentum could not be measured for a large number of tracks, especially for the events where an electromagnetic or hadronic shower develops already in the target region. To increase the momentum reconstruction efficiency, an additional set of tracker planes (Honeycomb trackers) was inserted during the last two years of data taking [38]. The hadron spectrometer, using the hits from both diamond tracker planes and honeycomb chambers, can reliably determine the charge for hadrons with momenta up to 10 GeV/c. To extend this range up to 30 GeV/c an emulsion tracker (ET) was installed, consisting of the three modules indicated in figure 2.1. With this upgrade, the momentum resolution is:

$$\frac{\Delta P}{P} = 22\% + 1\% \frac{P}{GeV/c} \tag{2.2}$$

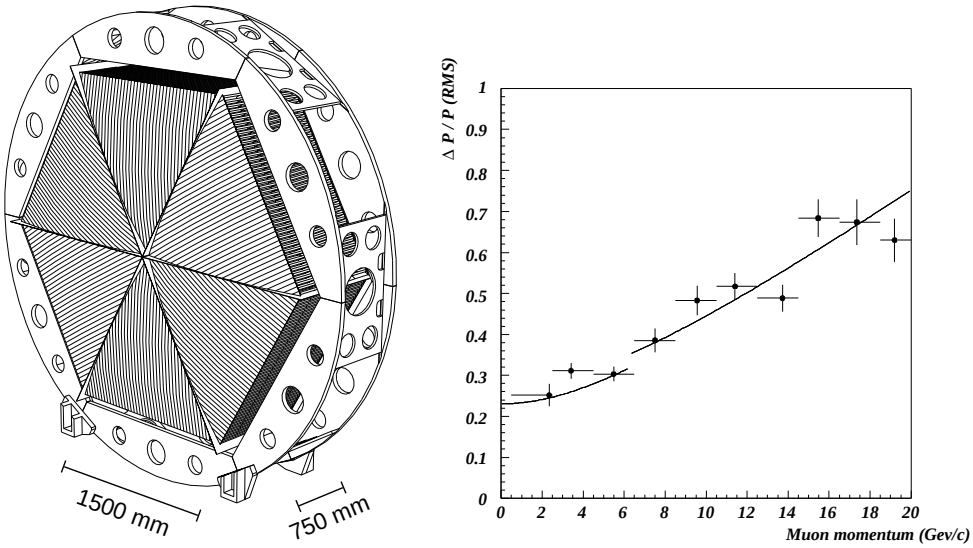

Figure 2.5: Left panel: drawing of the hexagonal air-core magnet. Right panel: resolution on the momentum measured by the magnet trackers for particles traversing the hexagonal magnet: the momentum measurement uses only diamond tracker information and the resolution was determined by comparing, in neutrino events, the momenta measured for muons which are also reconstructed in the muon spectrometer.

2.2.4 The calorimeter

The calorimeter had to measure the hadronic shower with sufficient energy and direction resolution. To facilitate the matching between trajectories reconstructed in the target tracker and in the muon spectrometer, the calorimeter should also have the capability to track through-going muons.

The CHORUS calorimeter [40] is longitudinally composed of three sectors of decreasing granularity, the electromagnetic sector (EM), the first hadronic sector (HAD1) and the second hadronic sector (HAD2). The first two sectors (EM and HAD1) are made of lead and scintillating fibres. It is the first large scale application of the calorimetric technique of embedding scintillating fibres into a lead matrix (the "spaghetti" technique). Scintillating fibres of 1 *mm* diameter and lead as passive material were chosen to assume both compensation[1] and good sampling, and consequently good hadronic energy resolution. The third sector (HAD2) is

[1]Compensation refers to the ratio between the response to electromagnetic and hadronic showers at the same energy; for a perfect compensation, this ratio would be one. In CHORUS calorimeter, the deviation from one is about 20%.

made of lead and scintillating strips (sandwich technique).

The total thickness of the calorimeter corresponded to about 150 radiation lengths or 5.6 hadronic interaction lengths. Therefore, most hadrons from neutrino interactions originating in the emulsion target were fully contained. The energy resolution for electrons amounted to:

$$\frac{\Delta E}{E} = \frac{(13.8 \pm 0.9)\%}{\sqrt{E(GeV)}} + (-0.2 \pm 0.4)\% \tag{2.3}$$

while for pions it is:

$$\frac{\Delta E}{E} = \frac{(32.3 \pm 2.4)\%}{\sqrt{E(GeV)}} + (1.4 \pm 0.7)\% \tag{2.4}$$

The constant term in the resolution function is related to instrumental effects, including electronic noise and broken modules, but dominated by intercalibration.

2.2.5 The muon spectrometer

The calorimeter absorbed most of the particles produced in neutrino interactions, except muons with momentum higher than 1.5 GeV/c. This provided their identification as muons, and the role of the muon spectrometer was to measure their trajectory, momentum and charge.

The main source of background for non-muonic tau decay is the neutrino induced charm production with the primary μ^- not reconstructed in the spectrometer. Thus, the CHORUS spectrometer performances affected in a very crucial way the sensitivity of the experiment.

The muon spectrometer consisted of six toroidal magnetised iron modules (shown in Fig. 2.6), instrumented with scintillating strips, drift chambers and streamer tubes. In addition, scintillating planes interleaved with the magnetised iron provided a measurement of the leakage of hadronic shower from the back of the calorimeter.

The particle position could be measured with a resolution of about 2.4 *mm*. The absolute calibration was performed by using negative 75 GeV/c test beam muons, corresponding to 71 GeV/c at the entrance of the spectrometer. The measured momentum resolution of the muon spectrometer was about 19%. The charge of stopping muons was determined by the curvature of the trajectory, whereas the momentum was determined by their range, resulting in a momentum resolution of 6% (Fig.2.6). The efficiency of the trigger signals provided by the spectrometer scintillators was close to 100%. The spectrometer energy resolution for shower tails above 1 *GeV* was $(110 \div 150)\%/\sqrt{E(\mathrm{GeV})}$.

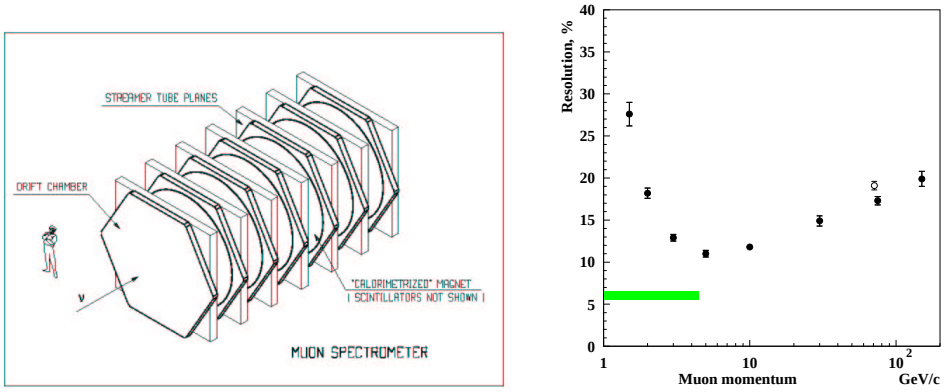

Figure 2.6: Left panel: Schematic view of the muon spectrometer. Right panel: momentum resolution as a function of muon momentum as evaluated from Montecarlo (full dots) and for 75 GeV/c test beam muons (open dot). The momentum of low energy muons stopping in the spectrometer was determined by range.

2.3 Nuclear emulsions

A nuclear photographic emulsion [41] consists of myriads of small crystals of silver halide with submicrometer linear dimensions embedded in gelatin. When ionising particles pass through it, some of the halide "grains" are modified in such a way that on immersing the plate in a reducing bath, called the "developer", they are turned into grains of silver which appear black. The final size of the grain and the distance between the initial ionisation point and the grain position mainly depend on the temperature, which is correlated to the diffusion of electrons and positive holes produced after ionisation, and on the development time, which affects the aggregation of silver atoms around the latent image.

The specific ionisation of a minimum ionising particle of charge $|e|$ is such that about 30 grains per 100 μm will be produced along its path. This number is sufficient to be distinguished under the microscope, and has to be taken into account by the automatic acquisition.

2.3.1 The analysis of nuclear emulsions

The excellent position resolution of nuclear emulsions allows detailed studies of the interaction and of the decay vertices, yielding measurements more accurate than any other detection system. Actually, nuclear emulsions integrate all charged tracks traversing them without time information, therefore a full reconstruction of the events cannot be performed by using only emulsions. For several decades,

emulsion analysis was fully visual, restricting their use to experiments with very low statistics due to highly time-consuming analysis.

The lack of time information was overcome by the design of hybrid experiments where nuclear emulsions and electronic detectors are used together. Hybrid experiments allow both triggering and kinematic reconstruction, as well as track and vertex reconstruction with very high degree of precision. The first hybrid experiment was E531 [28] at Fermilab in the 80's which analysed about 3000 ν_μ interactions by using a fully visual analysis: the statistics was limited by the analysis procedure.

A real revival of the emulsion technique occurred with the CHORUS experiment, thanks to the development of fully automatic scanning microscopes capable of analysing one event in 11 minutes. The hybrid technique with automatic scanning microscopes was also used by the DONUT experiment which provided the first direct observation of the tau neutrinos [43].

The CHORUS scanning procedure benefits of the impressive progress in automatic readout systems and the availability of fast data processing.

The emulsion scanning is performed by fully automatic microscopes optically connected with CCD cameras (with 512×512 *pixels* resolution and 120 *Hz* frequency) and a fast acquisition system, called Track Selector, developed at the Nagoya University [42], based on FPGAs and Pentium processors. The observed area is 90×120 μm^2 large. The last generation of automatic microscope is the UTS (*Ultra Track Selector*). Fig. 2.7 shows the UTS installed at Napoli laboratories.

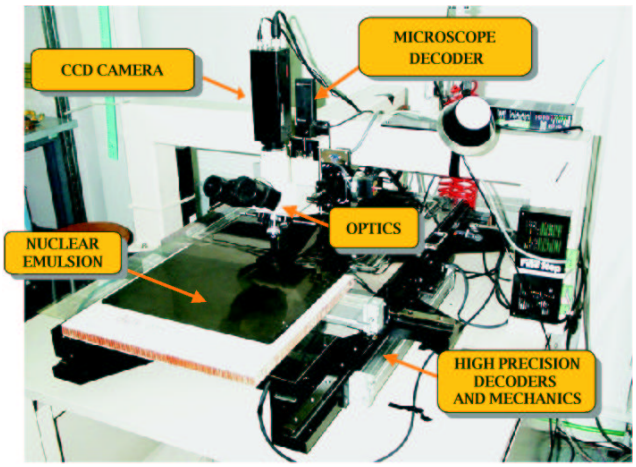

Figure 2.7: Picture of the UTS installed at Napoli.

Tracks inside the emulsions are identified and their parameters measured on

line. In order to recognise track segments in an emulsion plate, tomographic images are taken by focusing at different depths in the emulsion thickness. For each emulsion side, 16 layers at regular intervals of 3 μm are read, corresponding to the focal depth. The Track Selector video image processor digitises the CCD signals and sends the pixel of data into a dynamic frame memory. The 3D movement of the microscope is controlled by pulse motors with a linear encoder to an accuracy of less than 1 μm. A binarised image is formed by using the CCD pixel data, which in turns are clustered to grains. The tomographic image of in-focus grains at each depth is stored into each frame memory. After reading the images of all the layers, the digital signals are summed up as analogical signals, obtaining only one image with 16 grey levels. The grey intensity is called *pulse height*. In order to detect sloping tracks, the digitised images are regularly shifted one with respect to the other before the sum, either to record all tracks in the analysed emulsion area (*general angle scanning*) or according to the predicted track angle (*predicted angle scanning*). The most clear evidence of a track occurs when it forms hits (grains) at the same (shifted) position in each layer; the overlapped image presents a black cluster and the measured pulse height is 16. A cut on pulse height is done to reject background from random grains. The track detection efficiency is 98% for tracks with spatial angle up to 400 *mrad*. Fig. 2.8 shows a neutrino vertex as it appears in emulsions: black tracks are due to the nuclear fragmentation, the track search procedure used by the Track Selector is also schematically sketched.

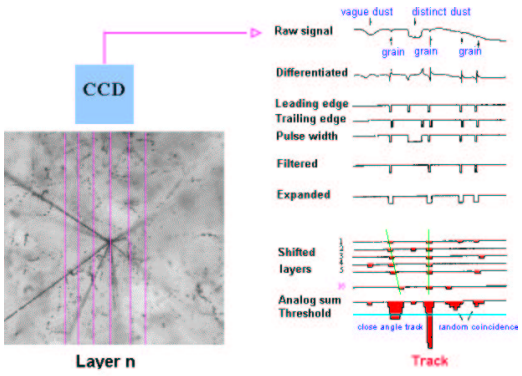

Figure 2.8: Track search procedure used by the Track Selector for a predicted track angle

Chapter 3

Event reconstruction in emulsions

The analysis strategy consists of four phases. In the first one the track reconstruction of electronic detectors is used to predict the event location in the emulsion target. The second step is the event location in emulsion: reconstructed tracks are scanned back through the emulsion target region until the vertex is located. In the third step, a fiducial volume around the vertex is analyzed by automatic microscopes and a tridimensional reconstruction of the neutrino interaction is produced; the events with a decay topology are selected. The last step is a computer assisted eye-scanning by well trained operators, in which the candidate events are carefully analyzed and validated. In this chapter these steps are described togheter with their Montecarlo simulation.

3.1 The reconstruction of neutrino interaction vertex by electronic detectors

All the events triggered and recorded in the electronic detectors are analyzed. These events are processed by the CHORUS reconstruction program to define the position of the primary neutrino interaction vertex and the parameters of the tracks exiting from it.

In the first phase of the CHORUS analysis (*Phase 1*) a reconstruction program named CHORAL was used to select the events for the emulsion analysis. In the second phase of the analysis (*Phase 2*), the CHORAL reconstruction program was replaced by the CHANT package, with more accurate track finding and fitting algorithms. We will describe shortly the most relevant selection criteria of the two phases, since the CHANT package did not replace CHORAL for the full event sample. The selection of candidate tracks to be used for the event reconstruction was based on a χ^2 matching probability in the angular and position variables. For all the events with a primary vertex reconstructed inside the emulsion stacks, the

track information is used to search for the interaction point in the emulsion target. Different criteria were applied to select the reconstructed tracks to be followed in the emulsions.

The following criteria were adopted during the *Phase 1* analysis:

- for events with a muon reconstructed by the electronic detectors, the muon track parameters provide the initial prediction for the vertex location procedure. In the first data analysis, only muons (negative and positive) with momentum less than 30 GeV/c were selected as scan-back track. To increase potentiality for charm search, in a subsample of events this momentum cut was removed;

- if more than one muon is reconstructed, no cut is applied and all reconstructed muons are followed up in emulsion;

- if no muon is recognized, all the negative hadrons with momentum in the 1 to 20 GeV/c range are kept as possible scan-back tracks.

The emulsion scanning of the event starts from the most downstream interface emulsion sheet, on the basis of the slope and position reconstructed by the Target Tracker (TT). All selected tracks (*scan-back tracks*) are searched for in the first interface sheet (the so-called *Changeable Sheet*, CS) closer to the electronic trackers. A rectangular area of 810×1080 μm^2 centered around the TT prediction is scanned. Each segment with an angular agreement better than 15 *mrad* in both projections is considered as a candidate and followed up in emulsions. If no track candidate is found, the event is rejected.

The track is then searched for in the *Special Sheet* (SS), which is closer to the emulsion stack, by observing the position and the direction measured in the corresponding Changeable Sheet. Due to the CS extrapolation accuracy, the rectangular area analyzed in the SS is smaller (630×840 μm^2). The track segments found in these sheets are then used to predict with high precision the position and the angle of the track in the emulsion stack.

A track found in both interface emulsion sheets is then followed upstream in the target emulsion stack from one plate to the next. In each plate only the most upstream 100 μm are scanned. The angular resolution is obtained by comparing the slope measured in each plate with the slope measured in the SS (see Fig. 3.1): $\sigma_y = 6.1$ *mrad*, $\sigma_z = 5.6$ *mrad*. The scanning area analyzed is 90×120 μm^2. The angular acceptance depends on the slope of the followed track: $\Delta\theta < (25 + 0.05 \cdot \theta_{SS})$ mrad. The tracking efficiency of the scanning system is 98%, therefore the probability to miss two consecutive plates is 0.04%. The scan-back track is stopped if the track is missing in two consecutive plates, the most downstream of which is defined as vertex plate (see Fig. 3.2).

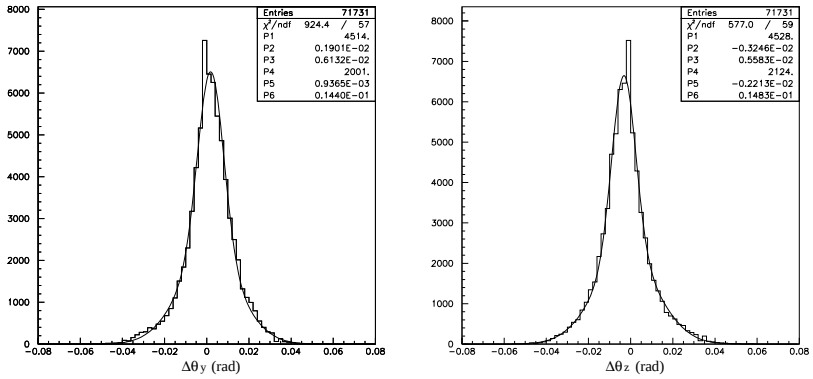

Figure 3.1: Slope difference between track measured in SS and track measured in bulk. The angular resolution is $\sigma_{\theta_y} = 6.1$ *mrad* and $\sigma_{\theta_z} = 5.6$ *mrad* for the two projections respectively.

The three most downstream plates of each stack are used to validate the matching between the TT prediction and the interface emulsion sheets. Therefore, events with the vertex in one of these plates are rejected.

For each event it is possible to find background tracks with slope and position similar to the scan-back track. They mainly originate from:

- halo muons associated with the neutrino beam and having its direction;
- muons from beams not related to the experiment (X7 and X9). The directions of these beams are clearly separate from the neutrino beam.

A fiducial volume cut is applied, rejecting all the vertices located within 1 *cm* from the border of each emulsion plate where the scanning would be very hard.

3.1.1 The event simulation

The CHORUS event analysis was simulated by Montecarlo techniques. The neutrino energy spectra was simulated, togheter with the neutrino interaction in the emulsion target. The outgoing particles were followed through the detector. A very detailed simulation of the vertex reconstruction in emulsion was performed.

The neutrino beam simulation

In order to optimize and predict the neutrino flux, the energy spectra and the beam contamination, a detailed simulation of the neutrino beam-line was performed

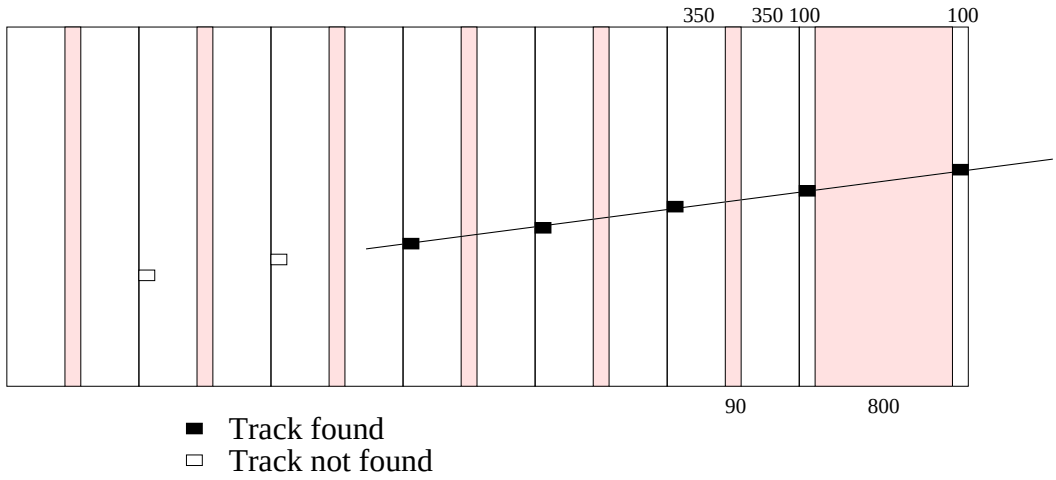

Figure 3.2: Vertex location procedure: the predicted track is followed up in the target emulsion stack by end. The vertex plate is defined as explained in the text.

[44, 45]. This simulation, called GBEAM2001, is GEANT based. It simulates the interaction of 450 GeV protons in the beryllium target and the hadronic shower all along the complete beam line.

Interactions of SPS protons with beryllium target and the production of secondary particles have been simulated by the NOMAD experiment [46] with a program based on the hadronic interaction generator FLUKA98 [47].

The propagation of secondary particles through the beam-line and their decays are simulated using GEANT [48]. The geometry and composition of all relevant elements in the beam-line are taken into account, as well as the magnetic fields in the horn and the reflector. For hadronic re-interactions downstream of the production target, the FLUKA98 interface was not available in GEANT. The GHEISHA package was used for the hadronic transport [48].

The neutrino beam mainly consists of muon neutrinos with a mean energy $\langle E_{\nu_\mu} \rangle \simeq 27\ GeV$. A muon anti-neutrino contamination mainly results from K^0 decays and from the remaining π^- component in the beam. The contamination of muon anti-neutrino is $\sim 5\%$ and the mean energy is $\langle E_{\bar{\nu}_\mu} \rangle \simeq 18\ GeV$. Electron (anti)neutrinos come mainly from semileptonic $K^\pm$ decays. An almost negligible prompt ν_τ component [29] is due to decays of D_s mesons produced in the production target and in the beam-dump. Fig.2.2 shows the simulated neutrino energy spectra.

The neutrino interaction with emulsion target

A specific event generator for neutrino interactions has been developed. Deep inelastic neutrino interactions, including charm production, are simulated by using the JETTA [49] event generator derived from JETSET [50], combined with LEPTO 6.1 [51] and TAUOLA [52]. The polarisation effects of the outgoing lepton are taken into account.

Quasi-elastic neutrino events and resonances are generated with RESQUE program. Nuclear effects such as Fermi motion and Pauli suppression are taken into account [53]. Nuclear re-interactions were not simulated.

The features of the beam simulation were studied by analysing the neutrino interactions in the calorimeter. An agreement at the 10% level on the relative $\bar{\nu}_\mu/\nu_\mu$ ratio has been found [54].

White kinks were simulated by the WHINTER [55] program, based on a detailed study of hadron interactions and the emulsion response. Several parameterisations obtained by FLUKA were introduced in this simulation program.

The detector response

The detailed simulation of the detector response was done by the EFICASS (Emulsion FIbers CAlorimeter and Spectrometer Simulation) program, based on the GEANT 3.21 package [48]. All primary tracks from the neutrino interactions in the detector were traced through the entire apparatus, taking into account all the relevant physics processes. A response was simulated for every particle crossing the sensitive volume of the detector. The simulated information is the same as for data, so that they can be processed with the same reconstruction programs.

The vertex location

The emulsion scanning of the scan-back tracks was simulated by using track segments produced by EFICASS. Position and slope acceptances used in CS, SS and bulk are the same as for data. Background tracks were simulated by using parameters extrapolated from emulsion data (see Ref. [56]). Since all tracks found in emulsion participate to the vertex location, background tracks increase the fraction of fake located events. This effect was evaluated to be less than 1% and it will be neglected. The angular resolution in the bulk was been introduced by producing angular smearing on the simulated track segments. The tracking efficiency of the scanning system was simulated by randomly rejecting 2% of the track segments found.

The reliability of the vertex location simulation was studied in the 1μ channel (see also Ref. [57]) by comparing located data with a Montecarlo sample including ν_μ and $\bar{\nu}_\mu$ simulated interactions, mixed according to the beam spectra. The

comparison with data was done by checking dependency on the most relevant parameters: the number of tracks reconstructed by the Target Tracker, the muon slope, the muon momentum and the calorimeter energy. The simulation (see Fig. 3.3) is in good agreement with data.

3.2 The Netscan procedure

Once the vertex plate has been identified, additional scanning is performed to analyze the event and identify short-lived particles. The very fast scanning system UTS makes a detailed analysis of the vertex point. For each event, all track segments within a given angular acceptance in a volume around the vertex position were recorded. We refer to this type of scanning, originally developed for the DONUT experiment [43], as *Netscan* data taking [58].

A sketch of Netscan volume is reported in Fig. 3.4. It is 1.5 *mm* wide in each transverse direction and 6.3 *mm* along the beam direction, corresponding to eight emlusion plates. It contains the vertex plate in the second upstream plate. The most upstream plate acts as a veto for passing through tracks. The six plates downstream of the vertex plate are meant for the particle tracking.

The scanning area is centered around the predicted position of the interaction vertex. The angular acceptance of the scanning is 400 *mrad* with respect to the beam direction. All located events are netscanned and all track segments recorded to perform the decay search. If at any stage during the vertex location there are multiple candidates, all of them will be followed up and vertex analysis will be performed independently, unless the fiducial volumes are closer than 100 μm.

3.2.1 Track and vertex reconstruction

The average number of straight tracks in one Netscan volume is about one hundred. Almost all of them are muons from X7 and X9 beams, particles produced in neutrino interactions further upstream not related to the event, and tracks due to low-energy particles. Most of them are passing-through tracks and are used to perform a precise alignment from one emulsion plate to the next. Due to the high spatial resolution of the emulsions, a plate-to-plate alignment has to be performed by comparing the pattern of segments in a plate with the corresponding pattern in the next upstream plate: all track segments found in the plate n are then extrapolated to the plate $n+1$ and compared with the measured segments in that plate. The comparison is performed also with the segments in the plate $n+2$. The matching is based on a χ^2 criterion. The passing-through tracks provide a sufficiently large sample of straight tracks to give a very precise alignment. The

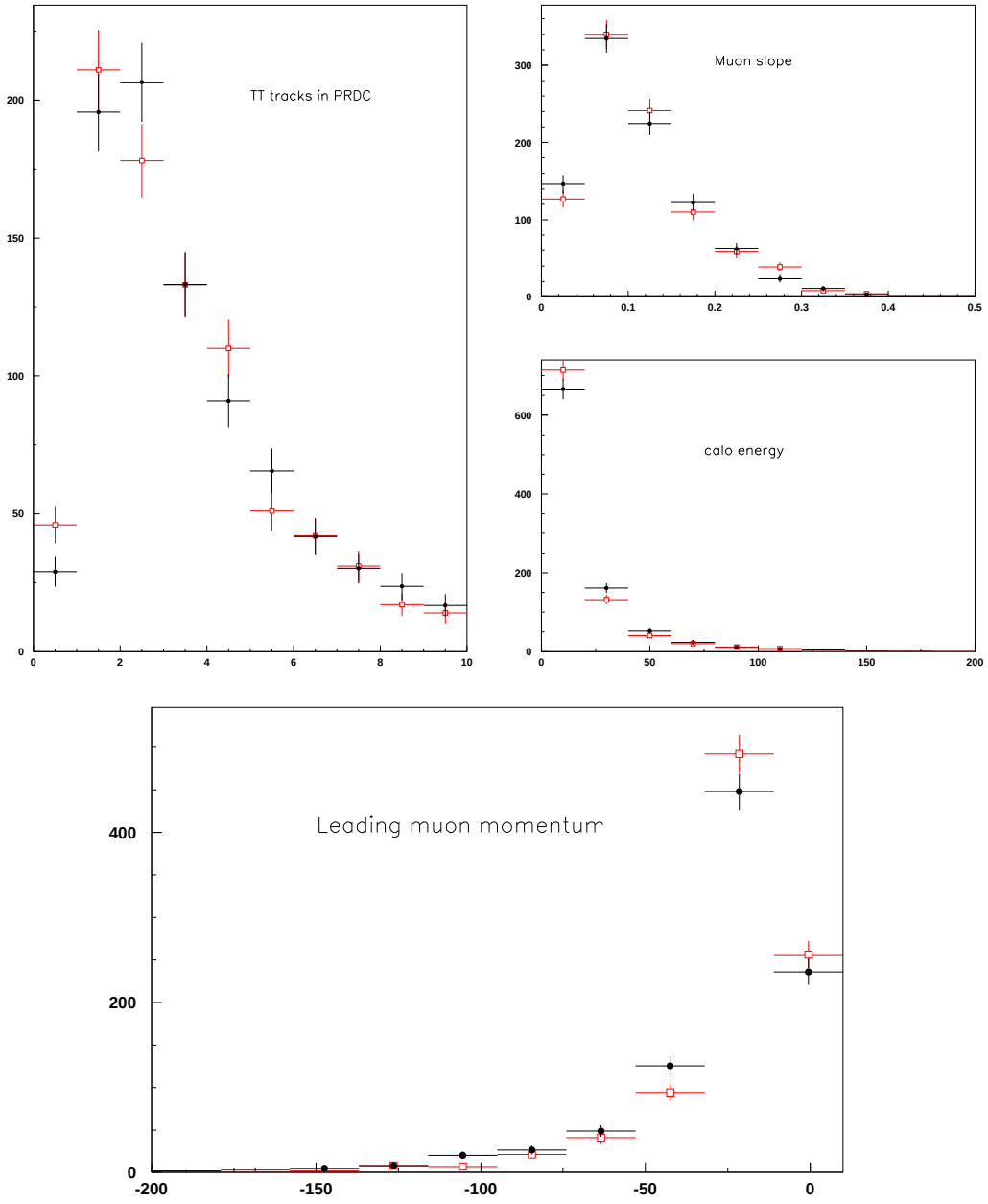

Figure 3.3: Located events distributions. Comparison between ν_μ CC data (empty circles) and simulated events (black points). Dependencies shown are the number of tracks reconstructed by the Target Tracker, the muon slope, the muon momentum and the calorimeter energy. Momentum was measured in GeV/c.

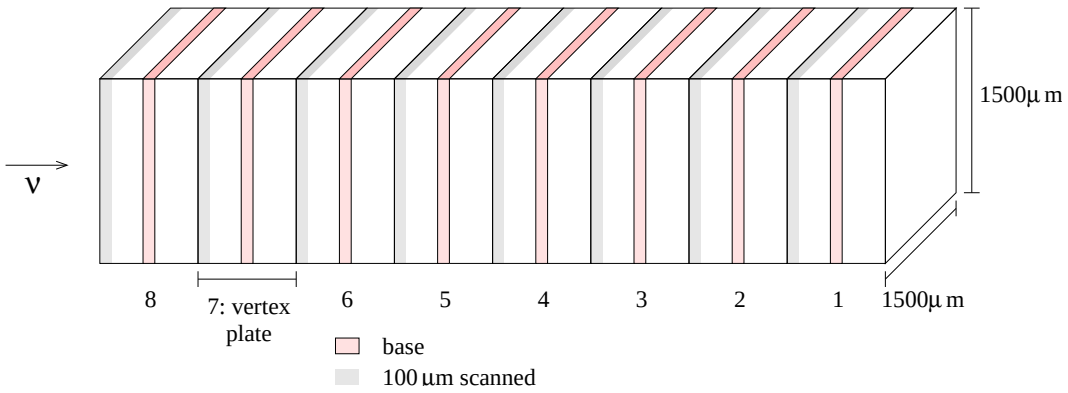

Figure 3.4: The scanning volume is 1.5 *mm* wide in each transverse direction and 6.3 *mm* along the beam direction.

number of connected tracks N (see Fig. 3.5) provides a good measurement of the alignment quality. If $N < 40$ the event is rejected.

In Fig. 3.6 the average position and slope residuals between the fitted tracks and the track segments are shown in three different angular ranges. If the position residual is $\sqrt{(\Delta y)^2 + (\Delta z)^2} > 1$ μm in the range $\theta < 100$ *mrad*, then the data-set is rejected.

After the alignment, passing-through tracks are rejected, as they are not correlated with the event. The background tracks due to low-energy particles are discarded on the basis of the goodness-of-fit for a straight line hypothesis and requiring at least two segments connected to define a track. After this preliminary track finding, about 40 tracks remain in the scanning volume. A more detailed description of the alignment and track finding algorithms can be found in Ref. [59].

After the tracking, reconstructed tracks are clusterized to make vertices, by means of the impact parameter for all combinations of tracks.

As the emulsions have no time information, to validate the reconstructed vertices a correspondence between emulsion tracks and tracks in the electronic detector is required. After the alignment of the coordinate system, the direction of emulsion tracks is compared with that of tracks from the electronic detector reconstruction by using a χ^2 criterion. A vertex is defined if at least one associated track is matched to a track given by electronic detector. Actually, two emulsion tracks can be matched to the same track in the electronic detectors or a single track can be attached to two different vertices. Such ambiguities are resolved again by means of χ^2 criteria.

At the end of the event reconstruction, we have a set of isolated tracks or tracks

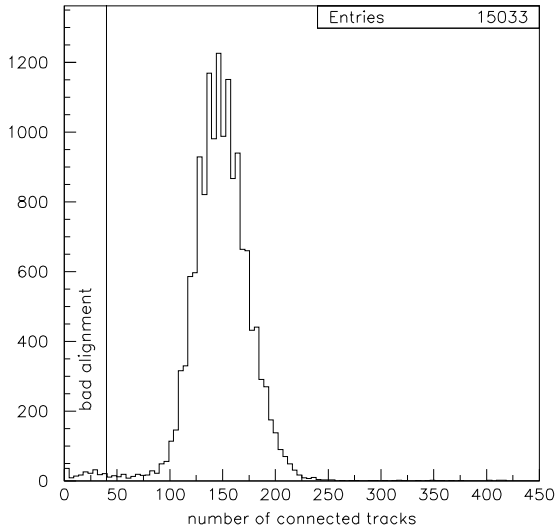

Figure 3.5: Number of connected tracks between the plate n and the plate $n+1$. If $N \geq 40$ the data-set is aligned.

attached to a vertex and one or more of these tracks are matched to the electronic detectors, all in an unique way. If the scanback track is recognized in the Netscan volume, the event is considered as *located*.

Table 3.1 shows the number of located events without any reconstructed muon (0μ channel), divided in different categories according to the year and to the reconstruction program used.

Reconstruction program	Year	Located 0μ events
CHORAL	'96	13530
CHORAL	'97	10163
CHANT	'96	2804
CHANT	'97	4062
ALL		30559

Table 3.1: List of 0μ events located in emulsion.

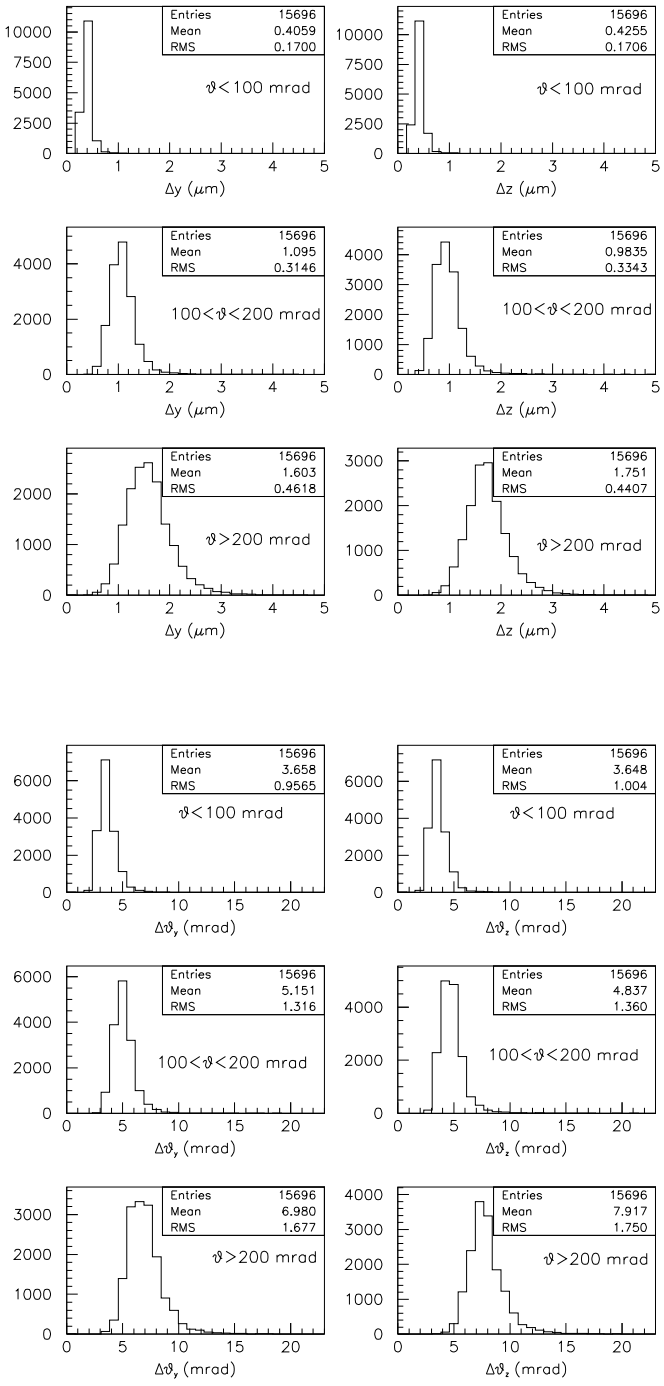

Figure 3.6: Average position and slope residuals between fitted tracks and track segments.

3.2.2 The Netscan procedure simulation

During the vertex location procedure, more than one track may be selected as scan-back track, or multi-candidates found in the interface sheets may be followed in the bulk emulsion. If these tracks stop in different emulsion plates, each of them is assumed to possibly contain a vertex and Netscan data taking is performed separately. If the scan-back track is fake, the scanned fiducial volume does not contain the neutrino interaction. Such data set is stored in the database and it is defined as an *empty data set*.

In the Netscan procedure, all track segments around the located vertex are recognized and there are a few thousand tracks in one Netscan acquisition for each event. These tracks originate from neutrino interactions, cosmic rays and other background tracks due to other beams during the exposure of CHORUS emulsions. In the real case, emulsion plates are misaligned one with respect to the other. Several hardware effects during the scanning procedure have to be taken into account. To evaluate the Netscan efficiency, all these aspects need to be reproduced. This was achieved by superimposing Montecarlo events with empty data sets. This is a very realistic way to simulate the background conditions in the Netscan procedure.

Starting from the Montecarlo true track parameters of all charged particles in a simulated neutrino interaction, each track is propagated from production point through the Netscan fiducial volume, taking into account the multiple scattering as well as the measurement error and the emulsion distortions, to get the position and direction of each track segment at the upstream surface of each plate. The number of frames (up to sixteen) where a grain is found, the so-called pulse-height, depends on the hardware efficiency. Using a large number of background tracks, the pulse-height distribution was parameterized as a function of the radial and transverse angle of the track, independently for each emulsion module. This parameterization was used to simulate pulse-height and took into account the hardware efficiency and the developing process that may result in different fog density and distortion [60]. Finally, to take into account the misalignment of the plates, the parameters of the inverse alignment transformation for the tracks in the empty data set are applied on the simulated segments to obtain segments in the same coordinate system as the raw data in the data set. In other words, misalignments are introduced for Montecarlo tracks using alignment parameters associated to scanned emulsion plates.

In doing so, the Montecarlo data set includes an event with known physical characteristics that can be treated in exactly the same way as real data. The combined data are passed through the same Netscan reconstruction and selection programs used for real data.

The ratio between the number of located events and the events interacting in

emulsion is called *location efficiency*. The table 3.2 shows the location efficiencies for the ν_τ signal and for backgrounds, composed of ν_μ *CC* with D^+, D_s^+, Λ_c^+ and D^0 charm production, and by ν_μ *NC* with white kink production. Also ν_μ *CC* events are shown. Tau and charm events are divided in different decay topologies. Events are also labeled as 1μ or 0μ. An event is 1μ if a muon is either found in the spectrometer or in the calorimeter. The simulated decay topologies are separated into three categories, also shown in Fig. 3.7: C1 and C3 are the one-prong and three-prong decays of a charged particle (also called kink and trident respectively), V2 is a two-prong decay of a neutral particle. White kinks simulate a C1 topology.

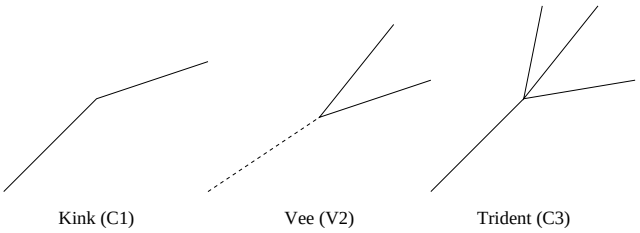

Figure 3.7: Decays topologies used in the analysis.

Event	Topology	Location efficiency (%)
ν_τ	$\tau \to e$	$\varepsilon_{loc\ 0\mu}^{\tau\to e} = 11.45 \pm 0.43$
ν_τ	$\tau \to h$	$\varepsilon_{loc\ 0\mu}^{\tau\to h} = 11.74 \pm 0.26$
ν_τ	$\tau \to 3h$	$\varepsilon_{loc\ 0\mu}^{\tau\to 3h} = 16.12 \pm 0.54$
ν_τ	$\tau \to \mu$	$\varepsilon_{loc\ 0\mu}^{\tau\to \mu} = 3.27 \pm 0.24$
$\nu_\mu\, CC \to$ Charm	$C1$	$\varepsilon_{loc\ 0\mu}^{D\to C1} = 0.98 \pm 0.12$
$\nu_\mu\, CC \to$ Charm	$V2$	$\varepsilon_{loc\ 0\mu}^{D\to V2} = 1.717 \pm 0.088$
$\nu_\mu\, CC \to$ Charm	$C3$	$\varepsilon_{loc\ 0\mu}^{D\to C3} = 1.57 \pm 0.13$
$\nu_\mu\, NC$	White kink	$\varepsilon_{loc\ 0\mu}^{WK} = 13.01 \pm 0.23$
$\nu_\mu\, NC$		$\varepsilon_{loc\ 0\mu}^{NC} = 14.2 \pm 0.5$
$\nu_\mu\, CC$		$\varepsilon_{loc\ 1\mu}^{CC} = 34.7 \pm 1.0$

Table 3.2: Vertex location efficiencies for signal and background. *Charm* labels stand for any charmed hadron: D^+, D_s^+, Λ_c^+ and D^0. C1,V2 and C3 are the decay topologies.

3.2.3 Selection of decay topologies

In Fig. 3.8 a sketch of a ν_τ Montecarlo event inside the Netscan volume is shown: a ν_τ (not visible) interacts producing a tau and other particles. After three plates, the tau decays into three hadrons.

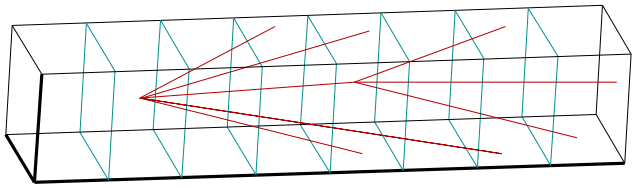

Figure 3.8: Montecarlo event inside the Netscan volume.

A selection criterion must recognize such process, even if some tracks are not detected. If a track is connected by angular matching to a Target Tracker track, it is called a *TT track*. If a track is connected to Target Tracker raw hits, it is called a *TThit track*. In both cases, this is a strong validation of the track. Two sets of selection criteria are used. The first set (let's call it selection A) was developed for charm search, but it was also used for tau search. It is composed of five selections:

- *Golden*. Two vertices are detected: the primary vertex and a secondary vertex with at least 2 TT tracks;
- *Silver*. Like the golden selection, but in this case only one TT track is reconstructed;
- *Par*. No TT track is found at the secondary vertex, but the decay parent track is detected;
- *Iso*. Only one vertex is found, but the scanback track (which is always a TT track) is a separate track;
- *SSt*. Only one vertex and one separate TT track are found.

The second set (selection B) is specifically optimized for tau search in the 0μ and one-prong decay channel. It is composed by four selections:

- *Short*. One vertex containing at least a TThit track and a isolate TThit track with an impact parameter (IP) in the range: $[7.2, 100]$ μm. This selection is very sensitive to short decays;

- *Long 1*. A kink is observed: one vertex containing at least a TThit track, one isolate TThit track and a short track connected with them (the parent track). The parent track has $IP < 6\mu m$ with the daughter one and $IP < 3\mu m$ with the vertex;

- *Long 2*. A multiprong decay is observed: two vertices each containing at least a TThit track are observed;

- *Long 3*. No vertex is present, but a kink topology is observed. The daugher is a TThit track.

3.2.4 The visual inspection of selected events

The events selected by at least one of these categories are then checked by visual inspection.

Emulsions allow the direct identification of short-lived particles through the visual observation of their decay. By changing the focal depth it's possible to follow track grains in emulsions and observe directly the interaction vertex and the decay point. All selected events are visually checked to confirm the presence of a secondary vertex and to measure accurately the position of the primary and secondary vertices, as well as all the tracks exiting from them.

In the majority of events, a neutrino interaction appears in emulsion as a star with outgoing shower tracks (from minimum ionizing particles) and some black tracks due to the nuclear fragmentation.

If the μ^- goes to the neutrino vertex interaction, the reconstructed most downstream vertex is checked to confirm the charm decay. Actually, secondary interactions or reconstruction artifacts can fake decay topologies.

Due to tracking inefficiencies, passing through tracks can be reconstructed as stopping. If the slope is compatible with a track in the electronic detectors, the event is selected. The visual inspection provides the possibility to follow the track in emulsion and to check if it goes to a genuine secondary vertices or if it is passing. δ rays, gamma conversions and low momentum tracks which, due to multiple scattering, are reconstructed as tracks with large impact parameter, can also be separate from genuine decay topologies by observing the tracks in emulsions. The distinction between hadronic interactions and decays can be performed by analyzing the secondary vertex point and the tracks exiting from it. Actually, an interaction is usually characterized by the nuclear fragmentation with the production of heavily ionizing particles and by the nuclear recoil visible as a blob at the interaction point. Moreover, since for hadronic interactions a visible charge conservation can be violated at a macroscopic level because of nuclear processes, it is possible to reject these events by checking the consinstency of the number of

prongs with the charge conservation. Nevertheless, hadronic interaction with no visible activity at the interaction vertex (white kink) may occur. This represents a not negligible background source and this is the reason for white kink interaction to be carefully simulated. The final data sample consists of 1210 tau candidates visually confirmed. Table 3.3 summarizes the results of visual scanning on the selected 0μ events and their topologies. In this table, also two-prong decays of neutral particles events (V2) are shown. Since such a decay topology cannot include tau decays, it was used to reduce systematics and to estimate the background for C1 and C3 samples.

	Selection A	Selection B	$A \cup B$
C1	37	48	60
V2	90	26	99
C3	37	31	50

Table 3.3: List of 0μ events selected by selection A and B and visually confirmed. The third column contains the bulk of events selected by at least one criterion.

3.2.5 Selection efficiencies

Netscanned simulated events are selected using the same selection algorithms used for data. The event is selected if tracks involved in the selection are true Montecarlo tracks belonging to the neutrino interacion. The *selection efficiency* is defined as the ratio between selected events and located events. Table 3.4 gives the selection efficiencies for signal and background. It also gives the overall efficiency (including the location efficiency) which will be used in the next chapter.

Event	Topology	Selection efficiency (%)	Overall efficiency (%)
ν_τ	$\tau \to e$	$\varepsilon_{sel\ 0\mu}^{\tau\to e} = 18.8 \pm 1.5$	$\varepsilon_{0\mu}^{\tau\to e} = 2.16 \pm 0.20$
ν_τ	$\tau \to h$	$\varepsilon_{sel\ 0\mu}^{\tau\to h} = 21.73 \pm 0.97$	$\varepsilon_{0\mu}^{\tau\to h} = 2.55 \pm 0.13$
ν_τ	$\tau \to 3h$	$\varepsilon_{sel\ 0\mu}^{\tau\to 3h} = 42.7 \pm 1.8$	$\varepsilon_{0\mu}^{\tau\to 3h} = 6.89 \pm 0.37$
ν_τ	$\tau \to \mu$	$\varepsilon_{sel\ 0\mu}^{\tau\to \mu} = 5.7 \pm 1.7$	$\varepsilon_{0\mu}^{\tau\to \mu} = 0.188 \pm 0.059$
$\nu_\mu\ CC \to$ Charm	$C1$	$\varepsilon_{sel\ 0\mu}^{D\to C1} = 18.6 \pm 4.6$	$\varepsilon_{0\mu}^{D\to C1} = 0.182 \pm 0.050$
$\nu_\mu\ CC \to$ Charm	$V2$	$\varepsilon_{sel\ 0\mu}^{D\to V2} = 33.4 \pm 2.4$	$\varepsilon_{0\mu}^{D\to V2} = 0.575 \pm 0.052$
$\nu_\mu\ CC \to$ Charm	$C3$	$\varepsilon_{sel\ 0\mu}^{D\to C3} = 47.2 \pm 4.1$	$\varepsilon_{0\mu}^{D\to C3} = 0.749 \pm 0.090$
$\nu_\mu\ NC$	White kink	$\varepsilon_{sel\ 0\mu}^{WK} = 5.71 \pm 0.43$	$\varepsilon_{0\mu}^{WK} = 0.748 \pm 0.058$

Table 3.4: Selection efficiencies and overall efficiencies for signal and background.

Chapter 4

The event analysis

In this chapter we report the study of signal and background events for the τ search in the 0μ decay channel. Charm data are used to control the reliability of the Montecarlo simulation. The analysis was applied to the 0μ data sample taken in the last two years of data taking. In order to increase the neutrino oscillation sensitivity, the signal to background ratio was improved. The analysis results of 0μ sample have been combined with data analyzed in the Phase I, to estimate the CHORUS oscillation limit in the $\nu_\mu \rightarrow \nu_\tau$ channel. The analysis proceeds in the following way:

- all background sources were examined and their yield estimated; a comparison with the data sample was done;
- dedicated post-scanning cuts were studied and applied to the MC signal and background; simulated events were divided into subsamples;
- the data was divided in the same samples and compared with the expected background. Each channel was statistically combined and the sensitivity and oscillation limit were derived.

4.1 Background evaluation in the 0μ channel

The hadronic and electronic τ decay channels are characterized by one or three prong decays in the 0μ sample. We report below the list of all physical processes, except τ decays, which show up as a kink (C1) or a trident (C3) decay topology after the visual inspection:

- C1: charm (D^+, D_s^+, Λ_c^+) decays, $\Sigma^\pm$ decay, "white" hadron interactions;
- C3: charm (D^+, D_s^+, Λ_c^+) decays, "white" hadron interactions;

We have to evaluate the yeld in each channel. In order to reduce the usage of MC simulation as much as possible, two-prong (V2) decays in the 0μ sample have been used. These events originate mainly from D^0 production in ν_μ *CC* events where the muon is misidentified. They are not background for the τ search since the parent track is neutral, but can be used to test the reliability of Montecarlo efficiency evaluation. Events which shows a V2 topology are mainly charm (D^0) with a small contribution of strange (K_s^0 and Λ^0) decays.

Another source of background is the ν_τ prompt component of the beam. The number of ν_τ *CC* interactions per ν_μ interactions is estimated to be $N_{\nu_\tau}/N_{\nu_\mu} = 3.3 \times 10^{-6}$ [29]. Since the total number of located ν_μ *CC* interactions in CHORUS is $N_{loc}^{CC} = 93890$, using the location efficiencies reported in the tables 3.2 and 3.4 and the following formula:

$$N_{\nu_\tau}^{\text{prompt}} = \frac{N_{\nu_\tau}}{N_{\nu_\mu}} \cdot \frac{N_{loc}^{CC}}{\varepsilon_{loc\ 1\mu}^{CC}} \cdot \sum_{i=1}^{4} BR(\tau \to i) \cdot \varepsilon_{sel\ 0\mu}^{\tau \to i} \quad i = \{e, h, 3h, \mu\}$$

we expect $N_{\nu_\tau}^{\text{prompt}} \lesssim 0.03$ events in the 0μ channel. These events are further reduced after additional post-scanning cuts showed in next sections. Their contribution is therefore negligible.

4.1.1 Strange particle decays

Neutrino interactions with $\Sigma^\pm$ production and subsequent decay mimic ν_τ interactions. Since the $\Sigma^\pm$ lifetimes are higher than for the τ, the probability to find a $\Sigma^\pm$ decay in the fiducial volume analyzed is small. However, it is not negligible. The events were simulated by using the full simulation chain in 1μ sample only [61], consisting of 93890 located events. The simulated decay topologies are:

- 1-prong
  $\Sigma^+ \to p\pi^0, n\pi^+$
  $\Sigma^- \to n\pi^-$

Since we use two-prong topology to estimate charm background in the C1 and C3 channels, also interactions with neutral strange particles production (K_s^0 and Λ^0) were simulated. They are:

- 2-prong
  $K_S^0 \to \pi^+\pi^-$
  $\Lambda^0 \to p\pi^-$

By assuming that the 0μ to 1μ channels ratio depends mainly by the number of decay prongs (shown in the table 4.1), we can derive this background component also in the 0μ sample. Table 4.2 shows the number of expected events.

	1μ	0μ	All	$0\mu/1\mu$ ratio
C1	470	37	507	0.081 ± 0.013
V2	883	90	973	0.103 ± 0.010
C3	536	37	573	0.071 ± 0.011

Table 4.1: List of candidate events for selection A divided in 0μ and 1μ subsamples.

	1μ channel	0μ channel
C1	8.6 ± 1.4	0.70 ± 0.16
V2	36.6 ± 3.5	3.77 ± 0.51

Table 4.2: Background contribution of $\Sigma^{\pm}$, K^0_s, Λ^0 in 0μ and 1μ subsamples.

4.1.2 Charmed particle decays

The charm component (D^+, D^+_s, Λ^+_c and D^0) is one of the main components of background in the ν_τ search, since the flight length of charmed hadrons is similar to the τ, so selection criteria have similar efficiencies to detect the decay topology. Charm production in 1μ sample shows a muon originating from primary vertex and therefore does not mimic ν_τ interactions with $\tau \to \mu$ decay. On the contrary, when the muon is misidentified, charm production shows the same topology as ν_τ interactions.

ν_μ ineractions with charm production were simulated with the full Montecarlo simulation chain in the 0μ sample. The table 3.4 shows the overall efficiencies. In order to reduce systematic effects in the 0μ definition from MC simulation, the charm contribution in the 0μ sample was determined by using the V2 sample, consisting by 90 events (see table 4.1). Subtracting the number of non-charmed events shown in the table 4.2, we have $N_{V2} = 90 - 3.77 = 86 \pm 10$ D^0 events. Starting from N_{V2}, we estimate the number N_{C1} of expected charm events with kink or trident.

The following cross sections and branching ratios are used [62]:

- Cross sections

$$\sigma_{C^+} = (3.06 \pm 0.39)\%$$
$$\sigma_{D^0} = (2.97 \pm 0.24)\%$$
$$\sigma_{D^+}/\sigma_{C^+} = 0.347 \pm 0.054$$
$$\sigma^{DIS}_{D_s^+}/\sigma_{C^+} = 0.130 \pm 0.022$$
$$\sigma^{DIFF}_{D_s^+}/\sigma_{C^+} = 0.088 \pm 0.028$$
$$\sigma^{DIS}_{\Lambda_c^+}/\sigma_{C^+} = 0.370 \pm 0.069$$
$$\sigma^{QE}_{\Lambda_c^+}/\sigma_{C^+} = 0.065 \pm 0.025$$

- Branching ratios

$$BR(D^0 \to V2) = 0.578 \pm 0.052$$
$$BR(D^+ \to C1) = 0.673 \pm 0.067$$
$$BR(D_s^+ \to C1) = 0.643 \pm 0.064$$
$$BR(\Lambda_c^+ \to C1) = 0.667 \pm 0.067$$

Using the following formula we estimate the number N_{C1}:

$$N_{C1} = \frac{N_{V2}}{\varepsilon_{V2}} \cdot \frac{1}{BR(D^0 \to V2)} \cdot \frac{\sigma_{C^+}}{\sigma_{D^0}} \cdot \varepsilon_{C1}$$

$$\varepsilon_{C1} = \sum_i \frac{\sigma_{D^i}}{\sigma_{C^+}} \cdot BR(D^i \to C1) \cdot \varepsilon^{C^+}_{C1} = (1.20 \pm 0.24) \times 10^{-3}$$

$$\boxed{N_{C1} = \frac{86}{0.00575} \cdot \frac{1}{0.578} \cdot \frac{3.06}{2.97} \cdot 0.00120 = 32.0 \pm 8.7}$$

In the same way, the number N_{C3} of charm events with a trident topology is:

$$N_{C3} = \frac{N_{V2}}{\varepsilon_{V2}} \cdot \frac{1}{BR(D^0 \to V2)} \cdot \frac{\sigma_{C^+}}{\sigma_{D^0}} \cdot \varepsilon_{C3}$$

$$\varepsilon_{C3} = \sum_i \frac{\sigma_{D^i}}{\sigma_{C^+}} \cdot BR(D^i \to C3) \cdot \varepsilon^{C^+}_{C3} = (2.19 \pm 0.31) \times 10^{-3}$$

$$\boxed{N_{C3} = \frac{86}{0.00575} \cdot \frac{1}{0.578} \cdot \frac{3.06}{2.97} \cdot 0.00219 = 58 \pm 14}$$

4.1.3 "White" hadronic interactions

"White" hadron interactions are elastic or inelastic hadron interactions which show no visible recoil nor delta rays or Auger electrons.

In the emulsion they cannot be topologically distinguished from a decay. The WHINTER simulation program simulates "white" hadronic interactions showing one prong topology ("white kinks"). At CHORUS energies, the interaction length in emulsion is estimated to be $\Lambda_{WSK} = 2.5 \pm 0.5$ *m*, by using FLUKA simulation program (see Ref. [63]). In the 1μ sample the white kink background is almost negligible because the probability that the hadron is identified as muon is very low. In the 0μ sample white kinks produced after ν_μ *NC* interactions can mimic the τ decay and we need to evaluate it with Montecarlo simulation. White kinks were generated (see Ref. [55]) and processed through the full simulation chain.

Selection criteria reduce the white kink background since kinks with an angle smaller than 30 *mrad* are difficult to be recognized in emulsion. In order to reduce white kink background, the cut on kink angle $\theta_{kink} > 50$ *mrad* was applied. The number of selected events normalized to the number of ν_μ *NC* generated interacting in emulsions is $A_{WK} = (4.42 \pm 0.35) \cdot 10^{-5}$. The number of expected white kinks is:

$$N_{WK}^{C1} = \frac{N_{loc\ 0\mu}}{\varepsilon_{loc\ 0\mu}^{NC}} \cdot A_{WK} = 9.5 \pm 0.8$$

where $N_{loc\ 0\mu} = 30559$ is the number of located events in the 0μ sample (see Table 3.1). From 1μ sample studies, hadronic interactions in three-prong topology are estimated to be 11% respect to one-prong topology [61]. So, we have:

$$N_{WK}^{C3} = 1.05 \pm 0.12$$

Table 4.3 summarizes the expected background and the observed candidate events in the 0μ channel for the C1 and C3 samples. Also candidate events are shown.

channel	Charm	Interactions	Other decays	Total BG	Data
$0\mu\,C1$	32.0 ± 8.7	9.5 ± 0.8	0.70 ± 0.16	42.2 ± 8.7	37
$0\mu\,C3$	58 ± 14	1.05 ± 0.12	–	59 ± 14	37

Table 4.3: Expected background and observed data for the C1 and C3 samples in the 0μ channel.

4.2 Post-scanning analysis

The largest background source for the τ source in the 0μ sample comes from charm and white kink events. In this section we report the kinematical analysis used to further reduce the background.

4.2.1 DT momentum of kink daughter track

In one-prong decay the τ daughter has always negative charge. Charged charmed particles have a positive charge, so their one-prong decay products have positive charge as well. White kinks are produced by $\pi^{\pm}$, $K^{\pm}$ and protons, so their charge is not unique. The Diamond Tracker (DT) was used to measure the charge of the kink daughter by fitting the hyperplane hits and by measuring the curvature of the track through a magnetic field. The kink daughter emulsion track was connected with the TT track by angular matching, by applying a cut on residuals $\Delta_\theta < 25$ *mrad* (Fig. 4.1 shows the residual distribution in data). The connected TT track was used as prediction in the DT.

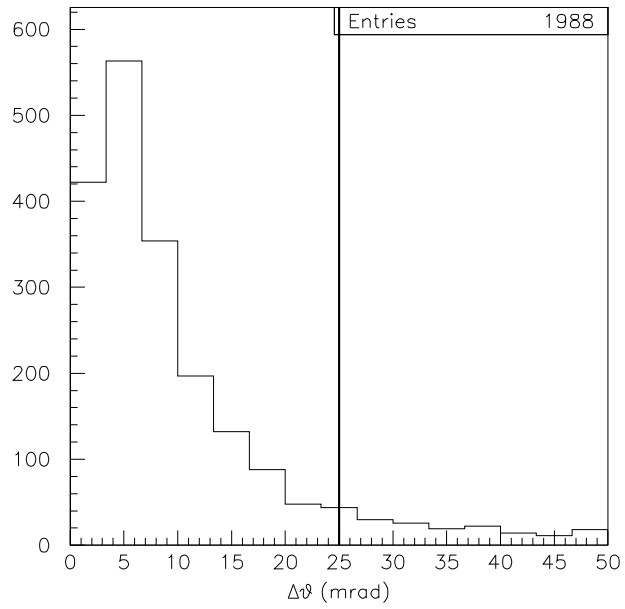

Figure 4.1: Angular residuals between emulsion tracks and TT track.

Charge and momentum are assigned to the track if a sufficient number of hits is found (a *rank r* is defined ranging from 0 to 6; the accepted rank is $r \geq 5$) and if the fit χ^2 probability is higher than 5%. A cut on momentum $1 < |P| < 20\ GeV/c$ was applied. In the Fig. 4.2 the rank, the fit probability and the momentum times charge distribution are shown.

The kink sample was divided into three subsamples:

- *No DT*: DT cannot measure the charge;
- *Yes DT, Charge -*: DT measure a negative charge;
- *Yes DT, Charge +*: DT measure a positive charge;

Table 4.4 shows the Montecarlo results for τ, charm and white kink events in the C1 channel. In the last column the results for data with V2 topology are shown, by using only one daughter track. The probability to have DT information is $(40 \pm 3)\%$, $(44 \pm 2)\%$, $(44 \pm 4)\%$ for charm, tau and WK Montecarlo samples, respectively. Simulation was not consistent with V2 data, where an efficiency of $(27 \pm 5)\%$ was found. The background was estimated by correcting Montecarlo results with data. The charge reconstruction efficiency is $(88 \pm 3)\%$ for the charm sample and $(88.0 \pm 1.6)\%$ for the tau sample.

	charm	tau	white kink	V2 data
All	380	895	179	90
No DT	229	505	100	66
Yes DT	151	390	79	24
Sign -	17	344	46	
Sign +	134	46	33	

Table 4.4: Summary of DT analysis with Montecarlo: comparison between charm, tau and white kink.

4.2.2 Transverse momentum of kink daughter track

The study of transverse momentum in one-prong topology allows the reduction of the white kink background. White kinks show a small stransverse momentum P_T respect to the initial hadron direction. Fig. 4.3 shows the P_T distribution for Montecarlo selected events, obtained by the formula:

$$P_T = P_{DT} \cdot sin(\theta_{kink}),$$

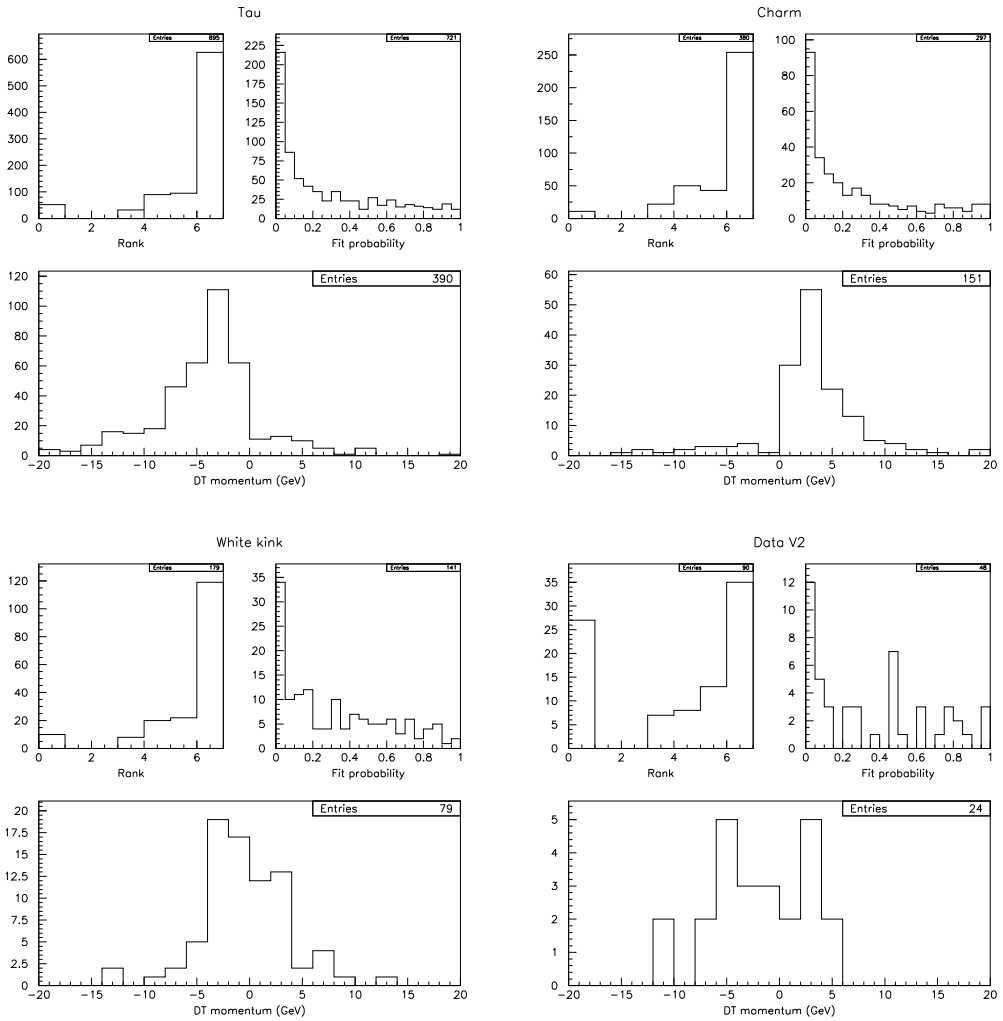

Figure 4.2: Rank r, fit χ^2 probability and momentum obtained by DT for τ, charm, white kink simulated events. V2 data are also shown by using one daughter track. χ^2 probability is shown for events with $r \geq 5$. The momentum distribution is shown for events with $r \geq 5$ and $P(\chi^2) > 5\%$.

where P_{DT} is the momentum measured by the DT and θ_{kink} is the kink angle measured in emulsion by visual inspection. The distributions are given with the $\theta_{kink} > 50$ *mrad* cut.

In order to reduce the white kink background, a $P_T > 250\ MeV/c$ cut was applied. Only 37% of the white kinks survived this cut. One prong τ decays, on the other hand, shows a P_T ranging up to 1 GeV/c. The P_T cut reduces the τ sample to 82%. One prong charm decays are reduced to 71%.

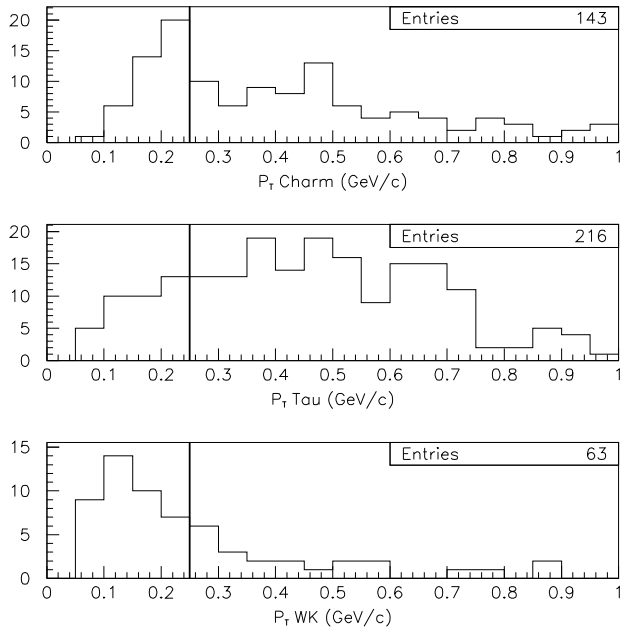

Figure 4.3: Transverse momentum computed in the charged charm, tau and white kink events of the C1 sample.

4.2.3 ϕ angle at the interaction vertex

In a charged current (CC) neutrino interaction, the charged lepton is produced back-to-back to the hadronic shower in the transverse plane. This is explained by the q^2 transferred from neutrino to the quarks inside the target nucleon via the W boson. In a ν_τ CC interaction the transverse momentum P_T of the τ lepton has opposite direction with respect to the average P_T of charged and neutral particles

produced in the interaction. In the transverse plane *xy*, the momentum components of a particle are:

$$P_x = P \cdot sin(\theta) cos(\phi)$$
$$P_y = P \cdot sin(\theta) sin(\phi)$$

where θ and ϕ are the polar and the azimuthal angle, respectively, respect to the beam direction *z*. At high energies, the momentum P is correlated with θ: $\langle P \rangle \propto \langle 1/sin(\theta) \rangle$. Then, the following approximation can be done:

$$\langle P_x \rangle \sim \langle cos(\phi) \rangle$$
$$\langle P_y \rangle \sim \langle sin(\phi) \rangle$$

Therefore, the average P_T vector has a weak dependency on the θ angle and on the absolute momentum P. It mainly depends on $(cos(\phi), sin(\phi))$ vector, i.e. on the particle direction in the transverse plane.

Unlike in the 1μ sample where charm production is always accompanied by a primary muon, charm production events where the muon is misidentified mimic τ events and therefore constitute a background source. However, the ϕ angle of the muon is opposite to the shower and roughly also to the charmed hadron. Let us define the $\Delta\phi$ variable as the difference between the ϕ angle of the decayed particle and the average ϕ angle of the shower tracks once we have removed from the shower the most far track with respect to the decayed particle (a sketch is shown in the Fig. 4.4). The $\Delta\phi$ variable can be used to discriminate τ events with respect to the charm background:

- In ν_τ interactions the decayed particle is the τ, then the most far track is a random shower track. Shower tracks are opposite to τ and $\Delta\phi$ is peaked at π;
- In ν_μ interaction with charm production the decayed particle is the charmed hadron. Since it carries the majority of the transverse momentum, its most far track is the muon (with about 95% of probability). Shower tracks have the same average direction of charmed hadrons and $\Delta\phi$ is peaked at 0;
- White kink in a ν_μ interaction is a random shower hadron interacting with the emulsion. In this case $\Delta\phi$ shows a flat distribution.

In emulsion, only charged tracks are detected. Then such behaviours become weaker. The location and selection criteria of neutrino events also modify the $\Delta\phi$ distributions. In Fig. 4.5 a comparison between ν_τ and charmed events in the C1 sample is shown.

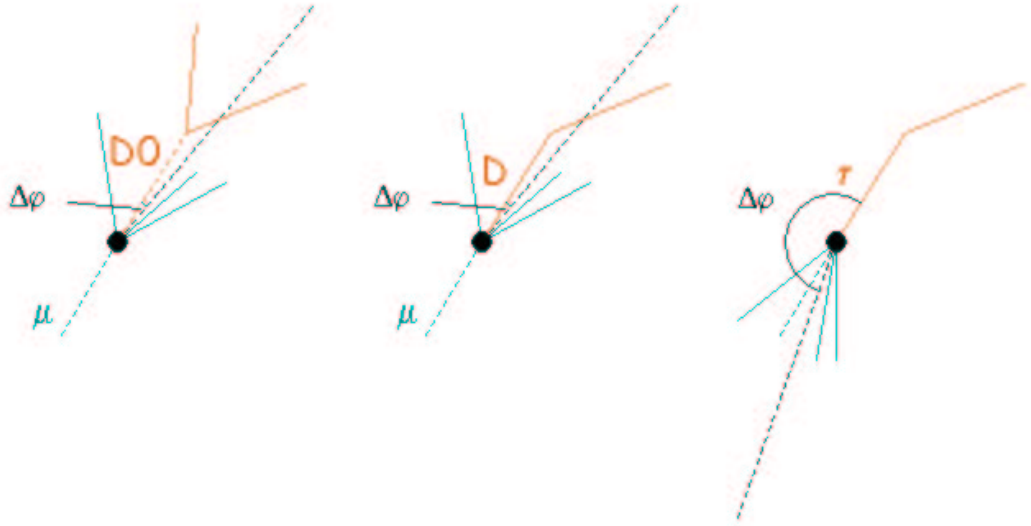

Figure 4.4: $\Delta\phi$ computed in the charged charm, neutral charm and tau events.

In order to use the $\Delta\phi$ variable, the selected candidate events were analyzed and angle of the tracks at primary vertex were measured. The high precision of the emulsion measurements makes the angular errors negligible. The reliability of the $\Delta\phi$ measurement was verified by comparing data and charm Montecarlo events for the V2 channel (see Fig. 4.6), which shows an agreement with $\tilde{\chi}^2_0 = 0.72$ (probability $P(\tilde{\chi}^2 \geq \tilde{\chi}^2_0)$ is 69%).

Finally data and background Montecarlo events were compared in the C1 and C3 samples (see Fig. 4.7), where the τ is expected. Background is obtained by combining charm and white kink events according to the predictions in Table 4.3. The $\Delta\phi$ distribution for neutral charm (V2) shows a peak at 0 higher than in the $\Delta\phi$ distribution for charged charms (C1 and C3). This is due to presence in the V2 sample of a relatively large fraction of D_0 produced by the D^{+*} resonance [64]. π^+ and D_0 produced by D^{+*} are emitted with a small angular difference, contributing to a small $\Delta\phi$.

In the final analysis all samples are divided into three subsamples according to the $\Delta\phi$ values. Table 4.5 shows their ranges and the signal to background ratio.

4.2.4 Lifetime of decayed particles

The τ lepton and the charmed particles have similar lifetimes. However, some discrimination can be performed on a statistical basis. In the table 4.6 the $c\tau$ is reported for τ and charged charm hadrons.

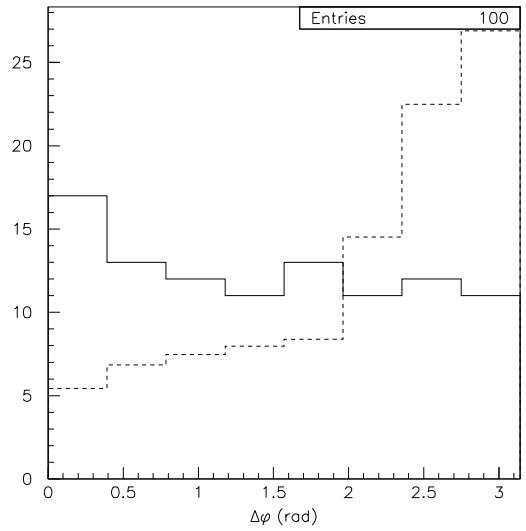

Figure 4.5: $\Delta\phi$ distributions: comparison between ν_τ (dashed line) and charmed events (solid line) in C1 sample.

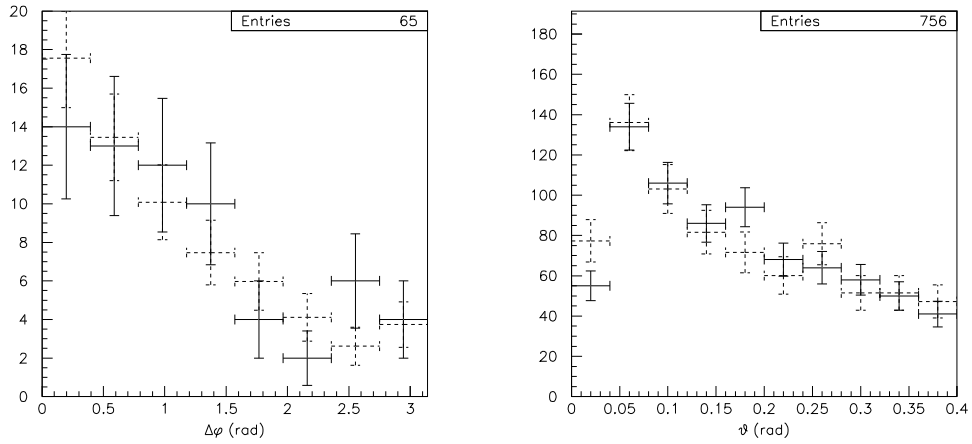

Figure 4.6: Comparison between data (solid line) and MC charm (dashed line) in V2 sample. Left: $\Delta\phi$ distribution. Right: spatial angle distribution of shower tracks.

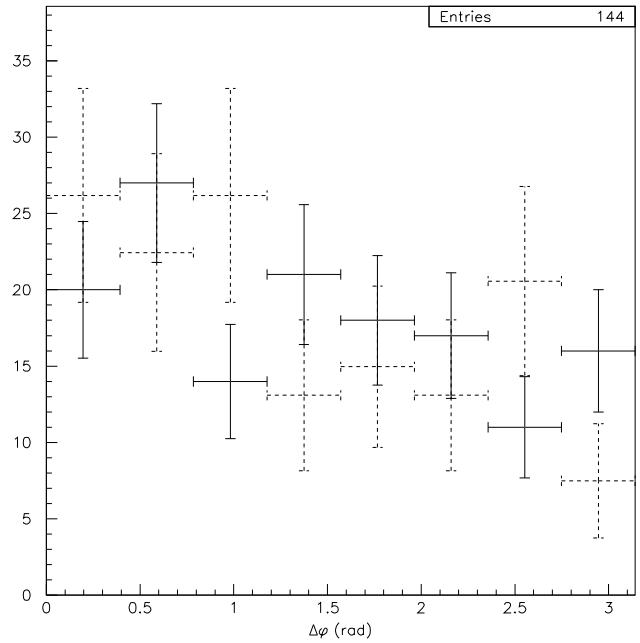

Figure 4.7: $\Delta\phi$ distribution: comparison between data (solid line) and MC charm (dashed line) in C1 and C3 samples.

$\Delta\phi$ range (rad)	signal/background
$[0;\pi/2]$	0.53
$[\pi/2;3\pi/4]$	0.94
$[3\pi/4;\pi]$	2.15

Table 4.5: Signal to background ratio into the three ranges of $\Delta\phi$ values.

	τ	D^+	D_s^+	Λ_c^+
$c\tau$ (μm)	87.11	311.8	147.0	59.9

Table 4.6: Lifetime of τ and charged charmed hadrons.

The average flight length (FL) of a short lived particle is related to its $c\tau$ through the equation $FL = \beta\gamma c\tau$. The γ variable is related to the opening angle of tracks produced after decay [65]. The faster the particle, the narrower the average opening angle $\langle\theta\rangle$. Since $\beta \sim 1$ and $\langle\theta\rangle \sim 1/\gamma$, the product $FL \cdot \langle\theta\rangle$ is a good variable to discriminate different lifetimes. Since only charged tracks can be detected in emulsion, this method is effective only when the number of prongs is high. For this reason, this study is applied only for the C3 sample. In the Fig. 4.8 is shown a comparison of $FL \cdot \langle\theta\rangle$ between τ and charged charmed events in the C3 sample.

The C3 sample was divided in "low $c\tau$" and "high $c\tau$", by using a cut on $FL \cdot \langle\theta\rangle = 75$ μm, also reported in the figure.

4.3 Maximum detectable τ's

The number of detectable ν_τ events if the oscillation probability is one (N_τ^{max}) is needed for the computation of the upper limit to the oscillation sensitivity. N_τ^{max} in the 0μ channel is calculated by using the following formula:

$$N_\tau^{max} = N_{loc}^{0\mu} \times \frac{\sigma_\tau^{CC}}{\sigma_\mu^{NC} \cdot \varepsilon_{loc\ 0\mu}^{NC} + \sigma_\mu^{CC} \cdot \varepsilon_{loc\ 0\mu}^{CC}} \cdot \sum_{i=1}^{4} BR(\tau \to i) \cdot \varepsilon_{0\mu}^{\tau \to i},$$

where $i = \{e, h, 3h, \mu\}$. $N_{loc}^{0\mu} = 30559$ is the number of located events in the 1996-1997 run period. The relative cross sections $\sigma_\tau^{CC}/\sigma_\mu^{CC} = 0.53$ and $\sigma_\mu^{NC}/\sigma_\mu^{CC} = 0.31$ were calculated by simulating of neutrino interactions with the CHORUS neutrino energy spectra. The location efficiencies for ν_μ CC and NC are shown in the table 3.2. The overall efficiencies for τ events are shown in table 3.4. Table 4.7 shows the branching ratios (BR) of the τ decays.

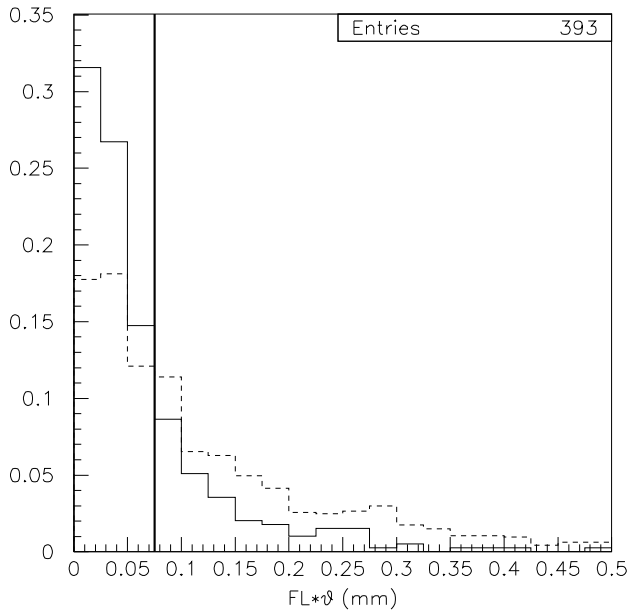

Figure 4.8: $FL \cdot \langle\theta\rangle$ distribution: comparison between τ (solid line) and charm (dashed line) decays in the C3 sample. Vertical line shows the applied cut $FL \cdot \langle\theta\rangle = 75\ \mu m$.

	$\tau \to h^-$	$\tau \to e^-$	$\tau \to 3h$	$\tau \to \mu$
BR(%)	49.5	17.8	15.2	17.4

Table 4.7: Branching ratios of τ decays.

Table 4.8 shows the number of expected ν_τ events for different decay topologies. The total number of ν_τ events is $N_\tau^{max} = 10034$.

	$\tau \to h^-$	$\tau \to e^-$	$\tau \to 3h$	$\tau \to \mu$	All decays
N_τ^{max}	4645	1415	3854	120	10034

Table 4.8: Expected number of ν_τ events in the 0μ sample.

4.4 Phase I results

The new data obtained in this work are the 0μ events collected during the 1996-1997 data taking, reanalyzed with the new techniques. In order to compute the upper limit to oscillation probability, they are combined with the results of Phase I analysis. The Phase I data have been divided into two samples:

- 1μ channel. The background reduction was obtained by applying a cut on the transverse momentum ($P_T > 250\ MeV/c$) of the kink daughter. The kink must also occur within five plates downstream of the neutrino inteaction vertex plate. The estimated background was of 0.1 events and the expected number of ν_τ events was $N_\tau^{max} = 5014$. No event was observed. The background is much smaller than 0μ sample because the probability of a wrong measurement of the charge in the muon spectrometer is low.

- 0μ channel of the 1994-1995 data taking. The estimated background was 0.3 events and the expected number of ν_τ events was $N_\tau^{max} = 526$. No event was observed.

4.5 Oscillation limit

The post-scanning analysis was used for background reduction in the data sample. Data can be divided into subsamples having different signal to background ratio, i.e. different sensitivity to neutrino oscillation. Table 4.9 shows the expected signal (N_τ^{max}) and background for each subsample. Also the 0μ sample for the 1994-1995 data and the 1μ sample of CHORUS Phase I were included.

DT infos	$\Delta\phi(rad)$	Background	N_τ^{max}	
$\tau \to 1\mu$		0.100 ± 0.025	5014	$*$
$\tau \to 0\mu\, C1$ [1994 – 1995 data taking]		0.300 ± 0.075	526	$*$
$\tau \to 0\mu\, C1$ [1996 – 1997 data taking]		42.2 ± 8.7	6180	
No DT	$[0;\pi/2]$	15.8 ± 3.1	1086	
	$[\pi/2;3\pi/4]$	5.1 ± 1.1	771	$*$
	$[3\pi/4;\pi]$	7.8 ± 1.9	2086	$*$
$P_T < 250\ MeV/c$	$[0;\pi]$	6.5 ± 1.3	689	
Charge -, $P_T > 250\ MeV/c$	$[0;\pi/2]$	0.67 ± 0.17	375	$*$
	$[\pi/2;3\pi/4]$	0.31 ± 0.07	266	$*$
	$[3\pi/4;\pi]$	0.39 ± 0.12	566	$*$
Charge +, $P_T > 250\ MeV/c$	$[0;\pi/2]$	2.8 ± 1.0	109	
	$[\pi/2;3\pi/4]$	0.86 ± 0.32	75	
	$[3\pi/4;\pi]$	1.98 ± 0.78	157	
$\tau \to 0\mu\, C3$ [1996 – 1997 data taking]		59 ± 14	3854	
Low $c\tau$ $(< 75\mu m)$	$[0;\pi/2]$	13.6 ± 3.3	691	
	$[\pi/2;3\pi/4]$	7.3 ± 1.7	680	$*$
	$[3\pi/4;\pi]$	4.5 ± 1.1	1392	$*$
High $c\tau$ $(> 75\mu m)$	$[0;\pi/2]$	18.2 ± 4.4	301	
	$[\pi/2;3\pi/4]$	9.1 ± 2.2	278	
	$[3\pi/4;\pi]$	6.4 ± 1.5	512	

Table 4.9: 1μ and 0μ C1 and C3 samples divided in different subsamples. The star indicates lower background channels.

The C1 sample for the 1996-1997 data is divided into the three categories according to the DT information: “No DT”, ”Charge -” and ”Charge +”. A cut on $P_T = P_{DT} \cdot sin(\theta_{kink}) > 0.250\ GeV/c$ was applied where the momentum is measured (“Charge -” and “Charge +” in the table). Each channel is further divided into three subsamples according to the $\Delta\phi$ values. The most sensitive sample to τ signal consists of events with high $\Delta\phi$ and kink daughter with negative charge.

The C3 sample was divided in “low $c\tau$” and “high $c\tau$”, by using a cut on $FL \cdot \langle\theta\rangle = 75\mu m$. These two samples are also divided according to $\Delta\phi$ values. The most sensitive sample to τ signal corresponds to events with low $c\tau$ and high $\Delta\phi$.

The average sensitivity to the oscillation probability was obtained by using the frequentist statistical approach (the so-called *Feldman and Cousins unified approach* [66]). All the most sensitive samples are combined togheter, with the same prescriptions used by the NOMAD Collaboration [67]. The acceptance region of Ref. [66] becomes multi-dimensional, to handle the separate measurements. The

likelihood ratio used in Ref. [66] has been replaced in order to take into account the uncertainties resulting from the limited statistics of the Montecarlo samples.

Figure 4.9 shows the upper limit distribution at 90% $C.L.$ obtained, in absence of signal events, for 308 simulated experiments with the same CHORUS expected background [66]. The average value is $P_{osc} = 2.9 \times 10^{-4}$ which corresponds to the sensitivity to $\nu_\mu \to \nu_\tau$ oscillation probability.

Only the channels with lower background (shown in Table 4.9 with a star) will partecipate into the sensitivity evaluation. The ramaining channels would not add any additional information. Post-scanning cuts were applied to data and candidate event distribution is shown in Table 4.10.

DT infos	$\Delta\phi(rad)$	Background	Data
$\tau \to 1\mu$		0.100 ± 0.025	0
$\tau \to 0\mu\, C1$ [1994 – 1995 data taking]		0.300 ± 0.075	0
$\tau \to 0\mu\, C1$ [1996 – 1997 data taking]		42.2 ± 8.7	37
No DT	$[0;\pi/2]$	15.8 ± 3.1	16
	$[\pi/2;3\pi/4]$	5.1 ± 1.1	8
	$[3\pi/4;\pi]$	7.8 ± 1.9	6
$P_T < 250\ MeV/c$	$[0;\pi]$	6.5 ± 1.3	3
Charge -, $P_T > 250\ MeV/c$	$[0;\pi/2]$	0.67 ± 0.17	1
	$[\pi/2;3\pi/4]$	0.31 ± 0.07	1
	$[3\pi/4;\pi]$	0.39 ± 0.12	0
Charge +, $P_T > 250\ MeV/c$	$[0;\pi/2]$	2.8 ± 1.0	2
	$[\pi/2;3\pi/4]$	0.86 ± 0.32	0
	$[3\pi/4;\pi]$	1.98 ± 0.78	0
$\tau \to 0\mu\, C3$ [1996 – 1997 data taking]		59 ± 14	37
Low $c\tau$ $(< 75\mu m)$	$[0;\pi/2]$	13.6 ± 3.3	12
	$[\pi/2;3\pi/4]$	7.3 ± 1.7	5
	$[3\pi/4;\pi]$	4.5 ± 1.1	3
High $c\tau$ $(> 75\mu m)$	$[0;\pi/2]$	18.2 ± 4.4	6
	$[\pi/2;3\pi/4]$	9.1 ± 2.2	6
	$[3\pi/4;\pi]$	6.4 ± 1.5	5

Table 4.10: 0μ C1 and C3 data compared with expected background.

Table 4.11 shows the samples used for the statistical treatment, the expected signal and background and the candidate events in each sample.

The resulting 90% $C.L.$ upper limit on the two-generation oscillation probability is:

Samples		Background	Data	N_τ^{max}
$\tau \to 1\mu$		0.100 ± 0.025	0	5014
$\tau \to 0\mu\, C1$ [1994 – 1995 data taking]		0.300 ± 0.075	0	526
$\tau \to 0\mu\, C1$ [1996 – 1997 data taking]				
No DT,	$\Delta\phi = [\pi/2; 3\pi/4]$	5.1 ± 1.1	8	771
No DT,	$\Delta\phi = [3\pi/4; \pi]$	7.8 ± 1.9	6	2086
Charge -, $P_T > 250\ MeV/c$,	$\Delta\phi = [0; \pi/2]$	0.67 ± 0.17	1	375
Charge -, $P_T > 250\ MeV/c$,	$\Delta\phi = [\pi/2; 3\pi/4]$	0.31 ± 0.07	1	266
Charge -, $P_T > 250\ MeV/c$,	$\Delta\phi = [3\pi/4; \pi]$	0.39 ± 0.12	0	566
$\tau \to 0\mu\, C3$				
Low $c\tau$,	$\Delta\phi = [\pi/2; 3\pi/4]$	7.3 ± 1.7	5	680
Low $c\tau$,	$\Delta\phi = [3\pi/4; \pi]$	4.5 ± 1.1	3	1392

Table 4.11: Summary of background and data events in the lower background bins.

$$P_{osc}(\nu_\mu \to \nu_\tau) < 2.3 \times 10^{-4},$$

which corresponds to $sin^2 2\theta_{\mu\tau} < 4.6 \times 10^{-4}$ for large Δm^2. This result improves significantly the previously published limit ($P < 3.4 \times 10^{-4}$ [23]). Vertical line in figure 4.9 shows the upper limit obtained. This is lower than the sensitivity, since the number of observed events is smaller than the estimated background. In absence of signal events, the probability to obtain an upper limit of 2.3×10^{-4} or lower is 31%.

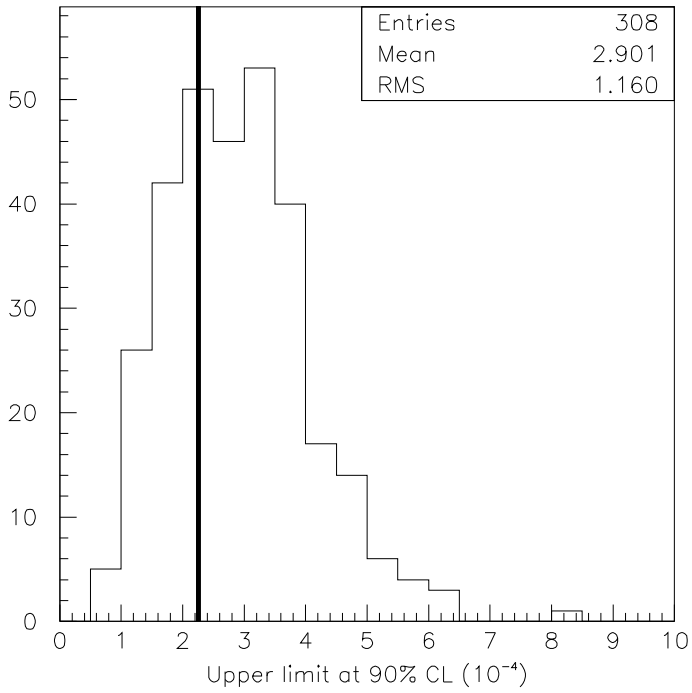

Figure 4.9: Upper limits obtained, in absence of signal events, for 308 simulated experiments with the same CHORUS expected background [66]. The average corresponds to the sensitivity to $\nu_\mu \rightarrow \nu_\tau$ oscillation probability. The vertical line is the upper limit obtained from data.

Conclusion

CHORUS searches for $\nu_\mu \rightarrow \nu_\tau$ oscillation in the appearance mode with the aim to reach high sensitivity in the mixing angle for values of the neutrino mass difference of interest in relation to the Dark Matter in the universe. The detector consisted by 800 kg active emulsion target, capable of observing the τ decay with a space granularity better than $1\mu m$. The downstream electronic detectors were responsible for the prediction of the track positions at the exit face of the emulsion and for the reconstruction of kinematic quantities. CHORUS data taking finished in 1998 and a first analysis was done. No signal event was observed and a limit on neutrino oscillation probability was given: $P_{osc}(\nu_\mu \rightarrow \nu_\tau) < 3.4 \times 10^{-4}$ at 90% C.L.

The CHORUS experiment provided a boost to the development of automatic scanning techniques and the speed has improved by an order of magnitude every three years over the past decade. In 2002 a new analysis started. A total number of $150,000$ interactions have been automatically located in emulsion. Furthermore, thanks to the increasing scanning capacity, the algorithms have gradually become more powerful and a wide range of physics can now be addressed, like charm physics. This new phase of analysis (*Phase II*) permits to increase the sensitivity to the neutrino oscillation probability; which was the aim of this work.

The features of the new analysis algorithms are presented. The analysis chain has been completely simulated and the efficiencies for all the τ decay channels obtained. A detailed analysis of all the background sources has been performed: charm and strange hadron decays, as well as *white* hadron interactions. Background reduction criteria are studied, based on kinematical and topological properties: charge, angle and transverse momentum of the decay products, momentum conservation at neutrino interaction vertex and average lifetime of the decayed particle. To apply such criteria, visual inspection of selected events in emulsion has been performed.

A further difference with respect to the Phase I analysis is the statistical approach used to estimate the sensitivity. The final result of the measurement is expressed as a frequentist confidence interval, dividing the event data set into subsamples, having a different signal to background ratio. This computation takes

into account the number of observed events, the expected background and its uncertainty, and the maximal number of the expected signal events. Such frequentist method is the so-called *Feldman and Cousins unified approach* using the same likelihood ratio definition as done by NOMAD.

The resulting 90% C.L. upper limit on the $\nu_\mu \to \nu_\tau$ oscillation probability is:

$$P_{osc}(\nu_\mu \to \nu_\tau) < 2.3 \times 10^{-4}$$

Under a two-neutrino family formalism this corresponds to $sin^2 2\theta_{\mu\tau} < 4.6 \times 10^{-4}$ for large Δm^2. This result is significantly more stringent than the previously published limit and constitutes the basis for the publication of the CHORUS final results.

Bibliography

[1] M.Fukugita and T.Yanagida, *Phys. Lett.*, **B174** (1986) 45;

M.Frigerio, *Phys.Atom.Nucl.*, **67** (2004) 1124.

[2] E.W.Kolb, M.S.Turner, The Early Universe, Addison-Wesley (1990).

[3] L3 Coll., M.Acciarri *et al.*, *Phys. Lett.*, **B431** (1998) 199.

[4] N.Cabibbo, *Phys. Lett.*, **B72**, (1978) 333.

[5] M.Frigerio and A.Y.Smirnov, *Nucl. Phys.*, **B640** (2002) 233 and *Phys. Rev.*, **D67** (2003) 013007.

[6] L. Wolfenstein, *Phys. Rev.*, **D17** (1978) 2369; S.P. Mikheev and A.Yu. Smirnov, *Yad. Fiz.*, **42** (1985) 1441.

[7] Homestake Collaboration, B.T. Cleveland, T. Daily, R. Davis Jr., J.R. Distel, K. Lande, C.K. Lee, P.S. Wildenhain, and J. Ullman, *Astrophys. J.*, **496** (1998) 505.

[8] SAGE Collaboration, J.N. Abdurashitov*et al.*, *J. Exp. Theor. Phys.*, **95** (2002) 181.

GALLEX Collaboration, W. Hampel *et al.*, *Phys. Lett.*, **B447** (1999) 127.

T. Kirsten for the GNO Collaboration, in Neutrino 2002, 20th International Conference on Neutrino Physics and Astrophysics (Munich, Germany, 2002).

[9] SK Collaboration, S. Fukuda *et al.*, *Phys. Lett.*, **B539** (2002) 179.

[10] SNO Collaboration, Q.R. Ahmad *et al.*, *Phys. Rev. Lett.*, **92** (2004) 181301.

[11] SNO Collaboration, Q.R. Ahmad *et al.*, *Phys. Rev. Lett.*, **87** (2001) 071301.

[12] SNO Collaboration, Q.R. Ahmad *et al., Phys. Rev. Lett.,* **89** (2002) 011302.

[13] CHOOZ Collaboration, M. Apollonio *et al., Phys. Lett.,* **B466** (1999) 415

[14] KamLAND Collaboration, K. Eguchi *et al., Phys. Rev. Lett.,* **90** (2003) 021802.

[15] G.L. Fogli, G. Lettera, E. Lisi, A. Marrone, A. Palazzo, and A. Rotunno, *Phys. Rev.* **D66** (2002) 093008.

[16] G.L. Fogli, E. Lisi, A. Marrone, D. Montanino , A. Palazzo, A.M. Rotunno, Talk given at Physics in Collision, (2003) hep-ph/0310012.

[17] T. Kajita and Y. Totsuka, *Rev. Mod. Phys.,* **73** (2001) 85.

[18] Soudan 2 Collaboration, W.W. Allison *et al., Phys. Lett.,* **B449** (1999) 137.

[19] MACRO Collaboration, M. Ambrosio *et al., Phys. Lett.,* **B517** (2001) 59.

[20] K2K Collaboration, M.H. Ahn *et al., Phys. Rev. Lett.,* **90** (2003) 041801.

[21] G.Altarelli and F.Ferruglio, hep-ph/0405048

[22] M. Guler *et al.,* OPERA experiment proposal, CERN/SPSC 2000-028 (2000)

M. Guler *et al.,* Status report on the OPERA experiment, CERN/SPSC 2000-028 (2001)

[23] CHORUS Coll., E.Eskut *et al., Phys. Lett.,* **B434** (1998) 205.

[24] NOMAD Coll., P. Astier *et al., Nucl.Phys.,* **B611** (2001) 3.

[25] CHORUS Coll., N. Armenise *et al.,* CERN-SPSC/90-42.

[26] CHORUS Coll., M. de Jong *et al.,* CERN-PPE/93-131.

[27] H.Harari, *Phys. Lett.,* **B216** (1989) 416 .

[28] FERMILAB E531 Coll., N.Ushida *et al., Phys. Rev. Lett.,* **57** (1986) 2897.

[29] B.Van de Vyver and P.Zucchelli, *Nucl. Instr. Meth.* **A385** (1997) 91.

[30] CHORUS Coll., P.Annis *et al., Phys. Lett.*, **B435** (1998) 458.
CHORUS Coll., E. Eskut *et al., Phys. Lett.*, **B503** (2001) 1.
CHORUS Coll., A.Kayis-Topaksu *et al., Phys. Lett.*, **B527** (2002) 173.
CHORUS Coll., A.Kayis-Topaksu *et al., Phys. Lett.*, **B539** (2002) 188.
CHORUS Coll., A.Kayis-Topaksu *et al., Phys. Lett.*, **B549** (2002) 48.
CHORUS Coll., A.Kayis-Topaksu *et al., Phys. Lett.*, **B555** (2003) 156.
CHORUS Coll., A.Kayis-Topaksu *et al., Phys. Lett.*, **B575** (2003) 198.
CHORUS Coll., A.Kayis-Topaksu *et al., Phys. Lett.*, **B596** (2004) 44.

[31] CHORUS Coll., E.Eskut *et al., Nucl. Instr. Meth.*, **A401** (1997) 7.

[32] G.Acquistapace *et al.*, CERN-ECP-95-014.

[33] CHORUS Coll., A.Kayis-Topaksu *et al., Eur. Phys. J.*, **C30** (2003) 159.

[34] M.G. van Beuzekom *et al., Nucl. Instr. Meth.*, **A427** (1999) 587.

[35] S.Aoki *et al., Nucl. Instr. Meth.*, **A344** (1994) 143.

[36] CHORUS Coll., P.Annis *et al., Nucl. Instr. Meth.*, **A367** (1995) 371.

[37] F.Bergsma *et al., Nucl. Instr. Meth.*, **A357** (1995) 243.

[38] J.W.E.Uiterwijk *et al., Nucl. Inst. Meth.*, **A409** (1998) 682.

[39] CHORUS Collaboration, S.Aoki *et al., Nucl. Instr. Meth.*, **A488** (2002) 144.

[40] S.Buontempo *et al., Nucl. Instr. Meth.*, **A349** (1994) 70.
E. di Capua *et al., Nucl. Instr. Meth.*, **A378** (1996) 221.

[41] P.H.Fowler, D.H.Perkins and C.F.Powell, The study of elementary particles by the photographic method. Pergamon Press (1959).

[42] S.Aoki *et al., Nucl. Instr. Meth.*, **B51** (1990) 446.

[43] DONUT Coll., K.Kodama *et al., Phys. Lett.*, **B504** (2001) 218.

[44] S.Sorrentino. GBEAM, the neutrino beam simulation. CHORUS Internal note 980056, May 1998.

[45] R.Oldeman. CHORUS Internal note 98001, March 1998.

[46] I.I. Tsukerman. Data vs MC comparison. CHORUS Internal note 2000010, September 2001.

[47] A.Fasso, A.Ferrari, P.R.Sala, *Electron-photon transport in FLUKA: Status* invited talk in the Proceedings of the MonteCarlo 2000 Conference, Lisbon, October 23–26 2000.

[48] *GEANT 3.21*. CERN program library long writeup W5013.

[49] P.Zucchelli. Calorimetric techniques for the kinematical selection of events in CHORUS. PhD thesis, Universitá di Ferrara (1995).

[50] T. Sjostrand. High-energy-physics event generation with PYTHIA 5.7 and JETSET 7.4. *Comput. Phys. Commun.*, **82**,74-90 (1990).

[51] G.Ingelman, Preprint TSL/ISV-92-0065, Uppsala Univ., May 1992

[52] Z.Was, *Comput. Phys. Commun.*, **76**,361 (1993).

[53] S.Ricciardi, PhD thesis, Universitá di Ferrara, 1996.

[54] R.G.C.Oldeman, PhD thesis, University of Amsterdam, June 2000.

[55] A.Satta, PhD thesis, Università degli studi di Roma “La Sapienza”, 2000

[56] L. Scotto Lavina, Laurea thesis, Università degli studi di Napoli “Federico II” 2001.

[57] G.De Rosa, Ph.D. Thesis, Università degli studi di Napoli “Federico II” 2003

[58] N.Nonaka, PhD thesis, Nagoya University, 2002.

[59] A.M. Guler, PhD thesis, Middle East Technical University, Ankara, 2000.

[60] M. Guler, O. Sato. Netscan Simulation. CHORUS Internal note 2000017, May 2002.

[61] M.Sorrentino, Università degli studi di Napoli “Federico II”, CHORUS Internal Note 2000027 (2004)

[62] G.De Lellis, P.Migliozzi, P.Santorelli, *Phys.Rept.*, **399** (2004) 227.

CHORUS Coll., A.Kayis-Topaksu, *et al.*, *Phys. Lett.*, **B555** (2003) 156.

[63] A.Fasso, A.Ferrari, P.R.Sala, *Proc. 3rd Workshop on Simulating Accelerator Radiation Environments (SARE 3)*, Ed. H.Hirayama (1997)

[64] CHORUS Coll., Paper in preparation.

[65] S.Petrera and G.Romano, *Nucl. Instr. Meth.*, **174** (1980) 61.

[66] G.J. Feldman and R.D.Cousins, *Phys. Rev.*, **D57** (1998) 3873.

[67] NOMAD Coll., P. Astier *et al.*, *Phys. Lett.*, **B453** (1999) 169.